Probing of nonlinear hybrid optomechanical systems via partial accessibility

V. Montenegro [1,*] M. G. Genoni [2,†] A. Bayat,[1,‡] and M. G. A. Paris [2,§]

[1]*Institute of Fundamental and Frontier Sciences, University of Electronic Science and Technology of China, Chengdu 610051, China*

[2]*Quantum Technology Lab & Applied Quantum Mechanics Group, Dipartimento di Fisica* Aldo Pontremoli*, Università degli Studi di Milano, I-20133 Milano, Italia*

(Received 6 January 2022; revised 27 April 2022; accepted 17 June 2022; published 13 July 2022)

Hybrid optomechanical systems are emerging as a fruitful architecture for quantum technologies. Hence determining the relevant atom-light and light-mechanics couplings is an essential task in such systems. The fingerprint of these couplings is left in the global state of the system during nonequilibrium dynamics. However, in practice, performing measurements on the entire system is not feasible, and thus one has to rely on partial access to one of the subsystems, namely, the atom, the light, or the mechanics. Here we perform a comprehensive analysis to determine the optimal subsystem for probing the couplings. We find that if the light-mechanics coupling is known or irrelevant, depending on the range of the qubit-light coupling, then the optimal subsystem can be either the light or the qubit. In other scenarios, e.g., simultaneous estimation of the couplings, the light is usually the optimal subsystem. This can be explained as light is the mediator between the other two subsystems. Finally, we show that the widely used homodyne detection can extract a fair fraction of the information about the couplings from the light degrees of freedom.

DOI: 10.1103/PhysRevResearch.4.033036

I. INTRODUCTION

The field of cavity quantum electrodynamics (QED) [1–3], as a rich blend of atomic physics and quantum optics, has led to countless striking applications, including the one-atom maser [4], one-atom laser [5], quantum gates [6,7], atom-cavity microscopy [8,9], and novel quantum information and computation schemes [10,11]. Undoubtedly, one of the most fundamental models to investigate the coherent interplay between atom-field interactions is the Jaynes-Cummings model (JCM) [12]. As initially formulated, the JCM is composed of a two-level atom interacting with a quasiresonant quantized cavity mode being first employed to unravel the classical aspects of spontaneous emission [13]. To date, numerous extensions of the original model have been put forward, for instance, in the presence of multiple atoms [14,15] and arrays of coupled cavities [16–18].

While JCM involves interaction between an atom and a bosonic field, the field of cavity quantum optomechanics [19–21] opens a new horizon by considering the interaction between two bosonic modes, namely, a quantized electromagnetic field and a mesoscopic mechanical resonator. The canonical formulation of the optomechanical model considers a nonlinear coupling between the photon number and the position of the mechanical resonator [22], making the physics of such systems inherently distinct from the linear (in the boson operator) nature of JCM. Similarly as for the JCM, the optomechanical systems have been also fully solved analytically for both time-dependent [23] and time-independent [24,25] Hamiltonians. Extensive experimental efforts and theoretical proposals have been devoted for the cooling of a mechanical object toward the ground state or even nonclassical states [26–50], which have led to a range of applications such as quantum state transfer [51], entanglement distillation [52], quantum state engineering [53], and quantum metrology purposes [54–60], to name a few.

Recently, cavity QED has been merged with optomechanics (see Fig. 1), enabling the emergence of vibrant novel hybrid systems [61–66]. Indeed, the nonlinear addition of a qubit into the optomechanical system allows us to simultaneously reach the strong single-photon optomechanical regime and the resolved sideband condition, a challenging experimental regime to reach in the absence of qubit hybridization [67,68]. While the constituent elements of cavity QED, i.e., the atoms and the light field, operate near resonance, the building blocks of optomechanics, i.e., the light and the mechanical fields, are highly off-resonant. Therefore the hybridization of quantum systems provide a rich playground for nonequilibrium dynamics involving distinct natural frequencies [61,68]. These versatile systems provide a fruitful architecture for various tasks for quantum technologies, including mechanical ground-state cooling [64,69–74], transducers for long-distance quantum communication [74–79], mechanical nonclassical state preparation [69,80], tunable photon blockade effects [81], quantum entanglement

*vmontenegro@uestc.edu.cn
†marco.genoni@fisica.unimi.it
‡abolfazl.bayat@uestc.edu.cn
§matteo.paris@fisica.unimi.it

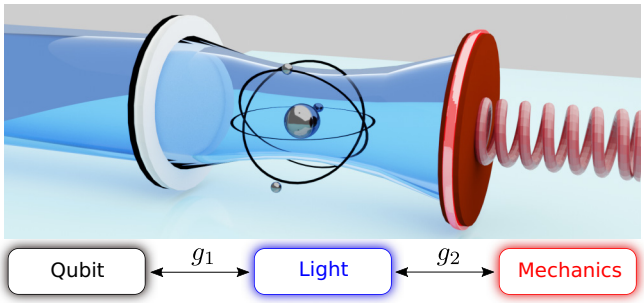

FIG. 1. Schematic of a hybrid optomechanical tripartite system. Two unknown parameters g_1 and g_2 are to be estimated in a cavity-mediated system with partial accessibility.

[66], and quantum nonlocality [82]. Thanks to recent advancements in quantum technologies, these structures have been proposed and realized in various physical platforms, resulting in a different range of couplings [83].

Consequently, the precise estimation of the couplings between the atom-light and the light-mechanics is a key step for harnessing the hybrid systems for practical applications. In order to approach this particular problem, we will then exploit the tools given by local quantum estimation theory (QET) [84–89] (for a global quantum sensing scheme see, e.g., Ref. [90]) whose aim is indeed to provide the ultimate bounds on parameter estimation in quantum systems and to assess the usefulness of practical measurement strategies. This kind of analysis has already been done for the estimation of Hamiltonian coupling constants both for light-matter interactions [91–93] and for optomechanical systems [94–97]. In general, as the system evolves, the information of the relevant couplings is imprinted in the quantum state of the global system [98,99]. To extract such information and estimate the parameters of interest, one must perform an appropriate measurement on the system. In practice, however, the accessibility to the whole system for performing a global measurement is unlikely. Therefore one has to resort to partial accessibility in which only one subsystem can be measured for inferring the information about the system. Since the dynamics make the subsystems of these hybrid structures highly entangled, the information contained in each of these subsystems is smaller than the global state. Indeed, quantum many-body sensors with partial accessibility show reduced sensitivity in spin chains, demanding complex driving necessary for restoring the precision [100,101]. Thus several issues should be addressed for probing the coupling in hybrid optomechanical systems by partial accessibility: First, how the information of the couplings spreads between the subsystems and how much of it can be extracted with partial accessibility; second, which subsystem has the maximum information content and thus is the best to be measured for estimating the couplings; third, by only considering the practically available measurements, which fraction of the information content can be experimentally extracted.

This paper addresses the above issues in a hybrid optomechanical system composed of a two-level atom, a cavity field, and a mechanical oscillator. The goal is to determine the couplings between the atom-light and the light-mechanics over a wide range, considering only partial accessibility to one of the subsystems. We consider three different regimes: (i) Estimating one coupling while the other is known (single-parameter estimation), (ii) estimating one coupling while the other is unknown (parameter estimation with nuisance parameters), and (iii) estimating both of the couplings simultaneously (joint estimation). For estimating the atom-light coupling, we found that in the single- and nuisance multiparameter estimation, depending on the range of couplings, either light or atom can be the optimal subsystem to be measured. In all other cases, the light is the dominant optimal subsystem to be measured. Surprisingly, measuring the mechanical degrees of freedom is hardly helpful for estimating the couplings. This can be understood as the light mediates the interaction between the other subsystems, thus carrying most of the information. Nonetheless, the optimal measurement basis on light degrees of freedom is very complex. Thus we focus on the widely available homodyne detection for the estimation of the couplings. Our analysis shows this can indeed determine the couplings simultaneously with fair precision.

The rest of the paper is organized as follows: In Sec. II we present preliminaries on quantum parameter estimation. In Sec. III we introduce the hybrid optomechanical model and a brief analysis on the entanglement dynamics. In Sec. IV, we address the single-parameter estimation scenario and the optimal subsystem which provides more information content. We present the multiparameter case in Sec. V, including nuisance and joint estimation protocols. We also investigate how much information one can extract with available homodyne detection schemes. In Sec. VI, we investigate the parameter estimation scenario in the presence of decoherence. In Sec. VII, we justify the chosen set of parameters with current state-of-the-art experiments. Finally, we conclude our work in Sec. VIII. An Appendix gives some analytical insight on the hybrid optomechanical system.

II. BITS OF QUANTUM PARAMETER ESTIMATION

In this section we will provide the basic ingredients of local QET (we refer to Refs. [84–87] for more details and explanations). We will start by considering the single-parameter case and we will then extend the formalism to the multiparameter one. We thus consider a family of states ϱ_λ, where λ is the parameter that one wants to estimate. In a quantum mechanical setting, one performs a measurement described by a positive-operator valued measure (POVM) $\{\Pi_x\}$, such that the whole process is described by the conditional probability

$$p(x|\lambda) = \mathrm{Tr}[\rho_\lambda \Pi_x]. \tag{1}$$

After obtaining a statistical sample of M outcomes $\mathcal{X} = \{x_1, \ldots, x_M\}$, one can then define an estimator $\tilde{\lambda}(\mathcal{X})$ to infer the value of λ. The variance of any unbiased estimator, such that $\mathbb{E}[\tilde{\lambda}(\mathcal{X})] = \lambda$, is proven to be bounded according to the Cramér-Rao bound

$$\mathrm{Var}(\lambda) \geqslant \frac{1}{MF}, \tag{2}$$

where we have introduced the (classical) Fisher information

$$F = \int dx \frac{1}{p(x|\lambda)} \left(\frac{\partial p(x|\lambda)}{\partial \lambda} \right)^2. \tag{3}$$

This bound can be in principle saturated via optimal estimators, such as the maximum likelihood or the Bayesian estimator. In quantum mechanics it is then possible to define a more general bound that depends only on the quantum statistical model ρ_λ and not on the particular measurement performed $\{\Pi_x\}$. In particular one proves the quantum Cramér-Rao bound

$$\mathrm{Var}(\lambda) \geqslant \frac{1}{MF} \geqslant \frac{1}{MQ}, \tag{4}$$

where we can now define the quantum Fisher information (QFI)

$$Q = \mathrm{Tr}\big[\rho_\lambda L_\lambda^2\big], \tag{5}$$

with the symmetric logarithmic derivative (SLD) operator L_λ implicitly defined by the Lyapunov equation

$$\frac{\partial \rho_\lambda}{\partial \lambda} = \frac{L_\lambda \rho_\lambda + \rho_\lambda L_\lambda}{2}. \tag{6}$$

Remarkably one can prove that the bound (4) can be always saturated, that is, one can always find an optimal POVM $\{\Pi_x\}$, such that the corresponding classical Fisher information F is equal to the QFI Q.

In the multiparameter scenario, the family of quantum states $\rho_{\boldsymbol{\lambda}}$ is defined in terms of a set of unknown d parameters $\boldsymbol{\lambda} = \{\lambda_1, \ldots, \lambda_d\}$. The bounds (2) and (4) can be generalized as matrix inequalities for the covariance matrix $\mathrm{Cov}(\boldsymbol{\lambda})$ of any unbiased estimator as

$$\mathrm{Cov}(\boldsymbol{\lambda}) \geqslant \frac{1}{M}\mathcal{F}^{-1} \geqslant \frac{1}{M}\mathcal{Q}^{-1}, \tag{7}$$

where we have introduced the classical and QFI matrices with elements

$$\mathcal{F}_{ij} = \int dx \frac{1}{p(x|\boldsymbol{\lambda})}\left(\frac{\partial p(x|\boldsymbol{\lambda})}{\partial \lambda_i}\right)\left(\frac{\partial p(x|\boldsymbol{\lambda})}{\partial \lambda_j}\right), \tag{8}$$

$$\mathcal{Q}_{ij} = \mathrm{Tr}\left[\rho_{\boldsymbol{\lambda}} \frac{L_i L_j + L_j L_i}{2}\right], \tag{9}$$

and where one defines a different SLD operator L_j for each parameter λ_j. The matrix bounds above can be translated into a family of scalar bounds, where in particular we will consider the one for the sum of the variances of each parameter

$$\sum_j \mathrm{Var}(\lambda_j) \geqslant \frac{1}{M}\mathrm{Tr}[\mathcal{F}^{-1}] \geqslant \frac{1}{M}\mathrm{Tr}[\mathcal{Q}^{-1}]. \tag{10}$$

One of the main differences between the single- and the multiparameter scenario is that, while the classical Cramér-Rao bounds (both matrix and scalar) defined in terms of the classical FI matrix $\mathcal{F}$ can be in principle saturated, this is not in general the case for the quantum Cramér-Rao bounds dictated by the QFI matrix $\mathcal{Q}$. This fact can be understood by observing that in general optimal measurements for different parameters may correspond to noncommuting observables. This led to the formulation of several other bounds that may be more tight under certain conditions [87]. However, in this work, we will not focus on this aspect, and we will rather consider the scalar bound (10) as an ultimate benchmark able to give relevant information on the multiparameter estimation properties of the quantum system under exam, and we will then focus on a particular feasible measurement strategy and to the corresponding (pontentially achievable) classical bound.

In the framework of multiparameter quantum estimation also falls the case of *nuisance quantum estimation* [102]: Suppose we are interested only in a single-parameter λ_j from the set of d unknown parameters $\boldsymbol{\lambda}$. In this case, the other $d-1$ parameters are typically called *nuisance parameters*, and the bound on the variance of any estimator of the parameter λ_j reads

$$\mathrm{Var}(\lambda_j) \geqslant \frac{1}{M}(\mathcal{F}^{-1})_{jj} \geqslant \frac{1}{M}(\mathcal{Q}^{-1})_{jj}, \tag{11}$$

where the inverse of the diagonal elements of the classical and QFI $F = \mathcal{F}_{jj}$ and $Q = \mathcal{Q}_{jj}$ in Eq. (4) have been replaced by the diagonal elements of the corresponding inverse matrices. One has that in general $(\mathcal{F}^{-1})_{jj} \geqslant (\mathcal{F}_{jj})^{-1}$ and $(\mathcal{Q}^{-1})_{jj} \geqslant (\mathcal{Q}_{jj})^{-1}$, confirming the fact that having less information on the other parameters can only lead to a worse estimation of the parameter λ_j. We, however, remark that in this case, the ultimate bound (11) for a single-parameter λ_j can be in principle achieved, with the optimal measurement strategy that coincides with the one that is optimal in the *nuisance-free* scenario.

As a technical remark, we point out that in order to derive the bounds described in this section, it is necessary to know the derivative of the operator respect to the parameters $\boldsymbol{\lambda}$, for example, in order to find the SLD operators as in Eq. (6). In our case, we will need to resort to numerical procedures often in order to evaluate this derivative. In particular we will compute the five-point stencil first derivative approximation with respect to λ_i and increment $\Delta\lambda_i \ll 1$:

$$\frac{\partial f(\lambda_i)}{\partial \lambda_i} \approx [-f(\lambda_i + 2\Delta\lambda_i) + 8f(\lambda_i + \Delta\lambda_i) - 8f(\lambda_i - \Delta\lambda_i) + f(\lambda_i - 2\Delta\lambda_i)]/(12\Delta\lambda_i), \tag{12}$$

which has an error of order $(\Delta\lambda_i)^4$.

III. THE MODEL

We consider a hybrid system composed of a two-level atom (qubit), a single electromagnetic (cavity) mode, and a (mechanical) harmonic oscillator. The qubit interacts with the cavity mode via JC Hamiltonian, whereas the cavity field couples to the mechanical oscillator through nonlinear optomechanical interaction [64]. Indeed, the qubit and the mechanical parties will interact with the cavity mode undergoing entirely different Hamiltonians. The total cavity-mediated tripartite Hamiltonian is ($\hbar = 1$)

$$H = \omega_c a^\dagger a + \omega_m b^\dagger b + \frac{\omega_q}{2}\sigma_z + g_1(\sigma^+ a + \sigma^- a^\dagger) - g_2 a^\dagger a(b^\dagger + b), \tag{13}$$

where the cavity (mechanical) mode is described by the bosonic operators satisfying $[a, a^\dagger] = \mathbb{I}$ ($[b, b^\dagger] = \mathbb{I}$) with natural frequency ω_c (ω_m). The qubit is described by Pauli matrices $\sigma_{x,y,z}$, $\sigma^+ = |e\rangle\langle g|$, $\sigma^- = |g\rangle\langle e|$ with energy-gap ω_q between the ground-state $|g\rangle$ and the excited energy level $|e\rangle$. The JC interaction term, $\sigma^+ a + \sigma^- a^\dagger$, accounts for the annihilation (creation) of a photonic excitation in the cavity by (de-)exciting the qubit ground state (excited state) with

coupling strength g_1. The nonlinear optomechanical Hamiltonian, $-g_2 a^\dagger a(b^\dagger + b)$, couples the cavity number operator directly to the mechanical object's position [$\propto (b^\dagger + b)$] via radiation-pressure interaction with strength g_2. While the diagonalization of the Hamiltonian in Eq. (13) for an arbitrary set of coupling strengths has not yet been found, the use of the polaron (a polariton-phonon states) basis permits diagonalizing the Hamiltonian for a particular regime of parameters [64,103]. For the sake of completeness, we present such diagonalization on a polaron basis as well as some needed analytical insights to grasp how the phononic excitations dress the polariton JC states in the Appendix A. We would like to estimate the coupling parameters g_1 and g_2 through the dynamics of the system when the accessibility to the system is limited, such that only one part of the hybrid system can be measured.

The JC Hamiltonian assumes $|\omega_q - \omega_c| \ll \omega_q + \omega_c$ for its derivation, which in turn allows us to neglect the fast temporal oscillations while keeping the rotating terms $\sigma^+ a$ and $\sigma^- a^\dagger$ [104]. As it is known, this rotating wave approximation holds valid when $g_1 \lesssim 0.1\omega_c$. Going beyond this regime, one necessarily needs to describe the dynamics with the isotropic quantum Rabi model as the counter-rotating terms $\sigma^+ a^\dagger$ and $\sigma^- a$ give rise to experimentally measurable effects [105]. The single-photon optomechanical coupling g_2 highly vary depending on the experimental setup considered [58]. Nonetheless, in the nonlinear regime its value range is typically from $g_2 \ll \omega_m$ to $g_2 \lesssim 0.2\omega_m$ for certain novel architectures [27,106–110]. In general $\omega_m \ll \omega_c$ and in what follows, we assume $\omega_c = \omega_q$ and $\omega_c = 100\omega_m$. Based on these, we consider the coupling g_1 and g_2 varying within a range $g_1 \in (0, 0.2\omega_m]$ and $g_2 \in (0, 0.2\omega_m]$.

We commence by considering the closed system evolution (the open quantum case is studied in Sec. VI) from the initial state:

$$|\psi(0)\rangle = |g\rangle \otimes |\alpha\rangle \otimes |\beta\rangle. \tag{14}$$

Here the qubit initializes in its ground-state energy, whereas the cavity (mechanical) field evolves from a coherent state of amplitude $\alpha = 2$ ($\beta = 2$). The system evolves under the action of the Hamiltonian as $|\psi(t)\rangle = e^{-iHt}|\psi(0)\rangle$. The quantum state of each subsystem is described by a reduced density matrix through tracing out the other parties

$$\rho_s(t) = \mathrm{Tr}_{\hat{s}}[|\psi(t)\rangle\langle\psi(t)|], \tag{15}$$

where the label s accounts for the cavity, qubit, or mechanical subsystems and $\mathrm{Tr}_{\hat{s}}[\cdot]$ means tracing out the complementary parts of the subsystem s. As the system evolves, the information of g_1 and g_2 is imprinted in the wave-function $|\psi(t)\rangle$, and thus $\rho_s(t)$. Regarding the estimation of g_1 and g_2, one can raise two open questions: (i) Which subsystem is more informative about the values of g_1 and g_2? (ii) What percentage of the global information content, extracted from the global state $|\psi(t)\rangle$, can be accessed through each subsystem? In the following sections, we address these issues.

Entanglement dynamics

The evolution governed by the Hamiltonian in Eq. (13) is complex and can only be solved analytically in the limit of vanishingly small g_2, namely, $g_2 \ll \omega_m$. Therefore for a general case we have to compute the evolution numerically. To understand the dynamics of the system, we investigate how each subsystem entangles in time, outlining relevant remarks on the tripartite correlation dynamics. To do so, we compute the von Neumann entropy

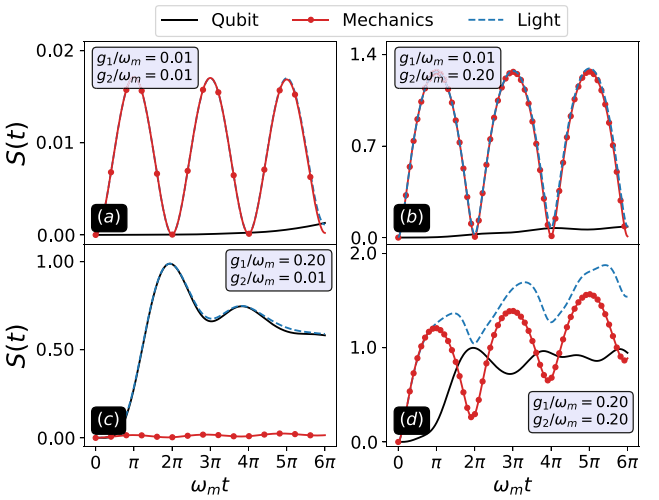

FIG. 2. Von Neumann entropy $S(t)$ for each subsystem as a function of the scaled time $\omega_m t$ for different g_1 and g_2 coupling parameters. The dynamics evolves from an initial state as in Eq. (14)

$$S(t) = -\mathrm{Tr}[\rho_s(t)\log_2\rho_s(t)], \tag{16}$$

which quantifies the degree of entanglement between the subsystem s and the rest of the system. Here the logarithm in base 2 sets the upper limit for a maximally entangled qubit subsystem as 1. Furthermore, we numerically truncate the cavity and the mechanical parties up to $n = 25$ of bosons, and hence one can fairly compare the entanglement between such subsystems. In Fig. 2 we compute the von Neumann entropy $S(t)$ for each subsystem as a function of the scaled time $\omega_m t$ for four representative g_1 and g_2 coupling parameters. In Fig. 2(a) we consider a regime where both g_1 and g_2 are small, namely, $g_1 = g_2 = 0.01\omega_m$. As the figure shows, each party weakly entangles with the rest of the system. However, a noticeable oscillatory entanglement of both the cavity and the mechanical oscillator within each mechanical cycle takes place. This is because the optomechanical interaction occurs in time scales of the order of $1/\omega_m$, while the qubit-light interaction, here scaled by ω_m, evolves in slower times proportional to $1/\omega_c$. In Fig. 2(b), we consider the situation where $g_2 \gg g_1$, namely, $g_2 = 0.2\omega_m$ and $g_1 = 0.01\omega_m$. As evident from the figure, the nonlinear optomechanical evolution dominates over the almost negligible qubit entanglement, showing the coherent light-matter dynamics due to the well-known nonlinear Kerr-like coherent phase [19,24]. The entanglement of the cavity and the mechanical oscillator takes its maximum at half of the mechanical oscillator's cycle [24]. Furthermore, one finds the expected mechanical disentanglement at multiples of $2\pi\omega_m t$, which due to the presence of the qubit, the disentanglement is only approximated. Note that in Figs. 2(a) and 2(b) the entanglement of the cavity and the mechanical oscillator follow an almost identical curve. This is because in these two regimes

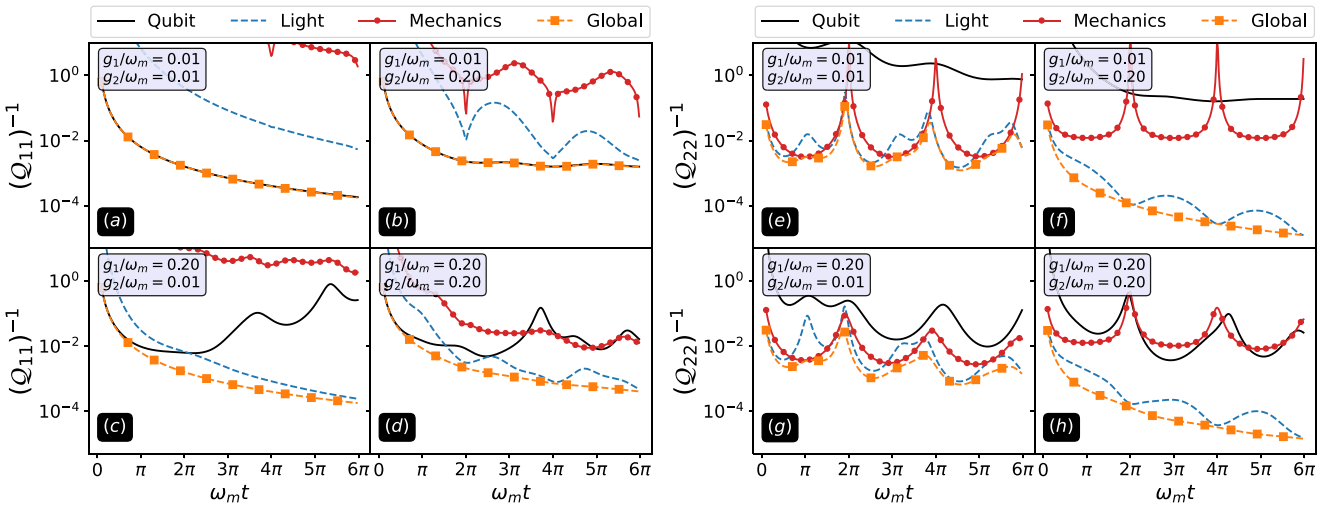

FIG. 3. Inverse of the QFI $(\mathcal{Q}_{ii})^{-1}$ for partial access and for the global state for four coupling parameters. Panels (a) to (d) show the estimation of g_1 by knowing g_2; panels (e) to (h) show the estimation of g_2 by knowing g_1.

g_1 is very small, and thus the qubit is almost disentangled from the rest. Therefore most of the entanglement is coming from the bipartite entanglement between the cavity and the mechanical oscillator. In Fig. 2(c), we consider the opposite regime where $g_1 \gg g_2$, namely, $g_1 = 0.2\omega_m$ and $g_2 = 0.01\omega_m$. Interestingly, the qubit (almost overlapped with the light subsystem) entangles maximally with the rest of the system at the first mechanical oscillator, remaining considerably high within the time interval $\omega_m t \in (0, 6\pi]$. This is because in this regime g_2 is very small, and thus the mechanical oscillator remains almost disentangled from the others. In Fig. 2(d), we consider a regime where both g_1 and g_2 are not negligible, namely, $g_1 = g_2 = 0.2\omega_m$. As opposed to the above cases, there is an evident interplay between parties, and thus one cannot only approximate its entanglement dynamics via JC or optomechanical Hamiltonians alone. Unlike Fig. 2(b), the stronger presence of the qubit makes the mechanical party remain entangled after one period. Additionally, it is observed that the qubit keeps highly entangled within the time window, whereas the mechanical and the light parties now entangle differently, with the cavity field reaching higher values of entanglement with the rest of the system. This analysis shows that, with partial accessibility, one has a rich playground for sensing g_1 and g_2 and depending on their values the most relevant subsystem may be different.

IV. SINGLE-PARAMETER ESTIMATION

Here we start to derive the different bounds on the estimation precision for the two coupling parameters. We will thus consider the evolved quantum state as our quantum statistical model $\rho_{\boldsymbol{g}}$, with the vector of parameters $\boldsymbol{g} = \{g_1, g_2\}$.

We first focus on setting the precision limits for estimating only one coupling parameter assuming the other one is known. As presented in Sec. II, in this case the ultimate bound is given by Eq. (4), and thus the expression that quantifies the above is $(\mathcal{Q}_{ii})^{-1}$, for $i = 1, 2$, and where $\mathcal{Q}$ is the QFI matrix corresponding to $\rho_{\boldsymbol{\lambda}}$.

In Fig. 3 we numerically evaluate the inverse of the QFI $(\mathcal{Q}_{ii})^{-1}$ for the partial and global states for four relevant coupling parameters.

Let us first focus on panels Figs. 3(a) to 3(d), where we show the precision limits in estimating g_1 by knowing g_2. In Figs. 3(a) and 3(c), we consider weak optomechanical coupling $g_2 = 0.01\omega_m$ while the qubit-light coupling takes the values $g_1 = 0.01\omega_m$ and $g_1 = 0.2\omega_m$, respectively. Notice that, while the quantum state can be derived as in Eq. (A11), the QFI expression remains intractable. Hence we rely on numerical simulations with the five-point method derivative as in Eq. (12). As expected, the mechanical oscillator which can encode g_1 only through the cavity field remains highly disentangled from the rest of the system due to small g_2 and thus plays an irrelevant role in estimating g_1. Nonetheless, as seen from Fig. 3(a), having partial access to the qubit subsystem nearly saturates the ultimate global bound. As g_1 increases, as shown in Fig. 3(c), a transition between the qubit and the light parties occur at $\omega_m t \simeq 2\pi$ for delivering the best partial estimation performance. Thanks to the regime of $g_2 \ll \omega_m$, the mechanical system can be neglected and the dynamics can be approximated by JC evolution. Indeed, an initial state $|\psi_{\rm JC}(0)\rangle = |g, \alpha\rangle$ evolves in the Schrödinger picture as

$$|\psi_{\rm JC}(t)\rangle = c_0|g, 0\rangle + \sum_{n=1}^{\infty} c_n(g_1)|g, n\rangle + d_n(g_1)|e, n-1\rangle, \tag{17}$$

where

$$\begin{aligned} c_0 &= e^{-|\alpha|^2/2}, \\ c_n(g_1) &= c_0 \frac{\alpha^n}{\sqrt{n!}} e^{-in\omega_c t} \cos(\sqrt{n} g_1 t), \\ d_n(g_1) &= -ic_0 \frac{\alpha^n}{\sqrt{n!}} e^{-in\omega_c t} \sin(\sqrt{n} g_1 t). \end{aligned} \tag{18}$$

The QFI for the JC global pure state in Eq. (17) can be derived analytically, yielding

$$(\mathcal{Q}_{11})^{-1}_{\rm global,JC} = 4|\alpha|^2 t^2, \tag{19}$$

which is almost equal to the precision achievable from the global state Fisher information, orange-squared line in Fig. 3. To observe that the global bound is nearly saturated by the qubit subsystem, one realizes that for weak qubit-light coupling $g_1 = 0.01\omega_m$ the system evolves approximately as

$$|\psi_{\rm JC}(t)\rangle \approx (|g\rangle + \theta(g_1)|e\rangle) \otimes |\alpha\rangle, \tag{20}$$

with a g_1-dependent coefficient $\theta(g_1)$. Obviously, all the information of g_1 is encoded in the state of the qubit, making it the most relevant subsystem to be used for sensing g_1. In short, the vanishing value of g_2 makes the mechanical part irrelevant and the small value of g_1 implies that the information is almost fully encoded in the state of the qubit. Note that Eq. (20) is only an approximation to have a qualitative understanding of the dynamics. For instance, although the cavity state in Eq. (20) looks independent of g_1, Fig. 3(a) clearly shows that the cavity subsystem carries information about g_1. On the other hand, increasing g_1, see Fig. 3(c), makes the Rabi coefficients $c_n(g_1)$ and $d_n(g_1)$ to dynamically encode the parameter g_1 into the cavity subsystem undergoing more complex dynamics as shown in Eq. (18). In Fig. 3(b), we consider $g_1 = 0.01\omega_m$ and $g_2 = 0.2\omega_m$. Again, similar to Fig. 3(a), because g_1 is small the information content of the qubit almost matches with the global state. However, since g_2 is large the mechanical state cannot be ignored anymore and one can write

$$|\psi(t)\rangle \approx (|g\rangle + \theta(g_1)|e\rangle) \otimes |\psi_{\rm OM}(t)\rangle, \tag{21}$$

where $|\psi_{\rm OM}(t)\rangle$ is the quantum state of the cavity and the mechanical oscillator evolved from $|\psi_{\rm OM}(0)\rangle = |\alpha, \beta\rangle$. By ignoring the JC Hamiltonian, one can show that (in a frame rotating at the frequency ω_c of mode a, thus ignoring the free evolution induced by the term $e^{-it\omega_c/\omega_m a^\dagger a}$) [24,25]

$$|\psi_{\rm OM}(t)\rangle = c_0 \sum_{n=0}^{\infty} \frac{\alpha^n}{\sqrt{n!}} e^{ig_2^2/\omega_m^2 n^2(\omega_m t - \sin(\omega_m t))} |n, \phi_n(t)\rangle, \tag{22}$$

where the coherent mechanical state evolves as

$$|\phi_n(t)\rangle = |\beta e^{-i\omega_m t} + g_2/\omega_m n(1 - e^{-it\omega_m})\rangle. \tag{23}$$

Obviously, the above is only an approximation as Fig. 3(b) clearly shows that the cavity and the mechanical states carry some information about g_1, although this is not evident in Eq. (22). In Fig. 3(d), we consider $g_1 = g_2 = 0.2\omega_m$. No approximation can be cast for this scenario. Interestingly, the cavity field is the subsystem which contains most of the information of g_1 and its achievable precision nearly reaches the ultimate global bound. Notice that for this regime, the mechanical oscillator also carries significant information about the coupling g_1, which is mediated through the cavity subsystem.

We now focus on panels Figs. 3(e)–3(h), where we examine the precision bounds in estimating g_2 by assuming we know g_1. In Figs. 3(e) and 3(f), we consider $g_1 \ll \omega_m$ with optomechanical values $g_2 = 0.01\omega_m$ and $g_2 = 0.2\omega_m$, respectively. In this case, the qubit system (which can encode g_2 only through the cavity field) plays an irrelevant role in the estimation of g_2 due to the very weak coupling g_1. In Figs. 3(e) and 3(f), the mechanics shows high peaks at $\omega_m t = 2\pi k$ for some integer k. This poor performance in estimating g_2 is because such a system almost returns to its initial state [see Eq. (23)] at those times,

$$|\phi_n(\omega_m t = 2\pi k)\rangle \approx |\beta\rangle, \tag{24}$$

and therefore it becomes almost completely independent of g_2. However, the mechanical system maximally entangles with the light field at $\omega_m t = k\pi$, which explains the constant lower bounds reached by the mechanics shown in Figs. 3(e) and 3(f). Notably, as g_2 increases the information content of the cavity field about g_2 reaches close to the global bound as evidenced in Fig. 3(f). Under the coarse optomechanical approximation, i.e., $g_1 = 0$, one can easily prove that accessing the light field coincides with the ultimate global bound at multiples of $\omega_m t = 2k\pi$, k being an integer. This is because at those times, the mechanical oscillator decouples from the light field and thus all the information of g_2 is transferred to the phase of the pure, decoupled cavity state. Indeed, from Eq. (22), one finds

$$(\mathcal{Q}_{22})^{-1}_{\rm global,opto} = (\mathcal{Q}_{22})^{-1}_{\rm light} = \frac{(|\alpha| g_2 k\pi)^{-2}}{64(1 + 6|\alpha|^2 + 4|\alpha|^4)}. \tag{25}$$

In Fig. 3(g), we consider $g_1 = 0.2\omega_m$ and $g_2 \ll \omega_m$. Here the strong presence of the qubit coupled to the cavity field prevents the mechanical oscillator to return to its original state, as evidenced in the attenuated peaks at $\omega_m t = 2\pi k$. In the regime where both g_1 and g_2 are strong, exemplified in Fig. 3(h) with $g_1 = g_2 = 0.2\omega_m$, accessing the cavity field delivers excellent performance in estimating g_2, almost saturating the global bound, in the presence of strong qubit-light interaction g_1.

In general, we can discuss the relationship between the entanglement of different subsystems and their related ultimate sensing precision by comparing the corresponding plots in Fig. 2 and Fig. 3, respectively. In particular, we observe very similar behavior in time, and specifically, a similar periodicity. On the one hand, we can understand how entanglement is necessary to redistribute the information on the parameters among the different subsystems. On the other hand, for entangled systems, the information on the parameters may be encoded in the (quantum) correlations between such subsystems, and as a consequence, one would lose this information by assessing only one of them. Indeed, as we also remarked before, we typically find that the optimal estimation precision typically corresponds to the local minima of entanglement: The subsystems acquire information on the parameters during the dynamics and such information is localized in these subsystems when the quantum correlations are small. The only scenario where this picture fails and one observes the opposite behavior is when one considers the estimation of the light-mechanical coupling g_2 via the mechanical system: We observe that the minimum of entanglement, observed at times $\omega_m t = 2\pi k$ in this case, typically corresponds to the worst estimation precision. This is because, at those specific times, the mechanical system almost returns to its initial state, and thus it carries little to no information on the parameter that can be extracted via a measurement on this subsystem alone.

Optimal subsystem

As discussed in the previous section, accessing different subsystems gives different estimation performances for a time

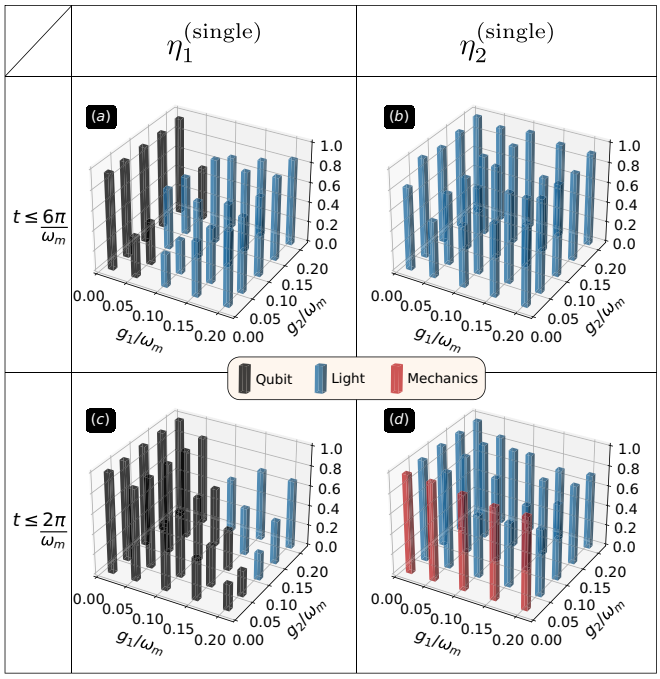

FIG. 4. Efficiency as defined as in Eq. (26) for the estimation of g_1 [panels (a) and (c)] and g_2 [panels (b) and (d)] for two time intervals. The height of each bar quantifies the performance with respect to the ultimate global bound, whereas the color for each bar represents the optimal subsystem.

interval and a given set of parameters g_1 and g_2. One can quantify the performance of each subsystem by comparing the $(\mathcal{Q}_{ii})^{-1}_{\mathrm{sub}}$ with the precision obtainable from the global state, namely, $(\mathcal{Q}_{ii})^{-1}_{\mathrm{global}}$. Therefore we define the single-parameter efficiency ratio

$$\eta_i^{(\mathrm{single})} = \left.\frac{(\mathcal{Q}_{ii})^{-1}_{\mathrm{global}}}{(\mathcal{Q}_{ii})^{-1}_{\mathrm{sub}}}\right|_{t=t^*}, \tag{26}$$

where t^* is the time where the optimal subsystem reaches its minimum within a given time interval. In general, $0 \leqslant \eta_i^{(\mathrm{single})} \leqslant 1$ and each subsystem which contains more information about g_i results in higher values of $\eta_i^{(\mathrm{single})}$.

By fixing the time within the interval $t \leqslant 6\pi/\omega_m$, we determine which subsystem achieves higher efficiency. In Figs. 4(a) and4(b), we depict the optimal subsystem as a function of g_1 and g_2. In Fig. 4(a), g_1 is estimated while g_2 is known. Interestingly, for small values of g_1, no matter what g_2 is, the optimal subsystem is the qubit. For $g_1 > 0.05\omega_m$, the optimal subsystem changes to be the light. In Fig. 4(b), g_2 is estimated while g_1 is known. Remarkably, the light remains the optimal subsystem for all ranges of g_1 and g_2. In practice, the time over which the estimation can happen is highly limited due to imperfections such as decoherence, damping, and dephasing. By reducing the time interval to $t \leqslant 2\pi/\omega_m$, we repeat the above analysis to determine the optimal subsystem. In Figs. 4(c) and 4(d), we depict the optimal subsystem as a function of g_1 and g_2. In Fig. 4(c), we consider the case where g_1 is estimated and g_2 is known. Interestingly, compared with Fig. 4(a), in most of the cases, the optimal subsystem becomes the qubit. In Fig. 4(d), we consider estimation of g_2 when g_1 is known. Surprisingly, compared with Fig. 4(b), in the regime that g_2 is very small, the optimal subsystem becomes the mechanical oscillator.

This analysis shows that the optimal subsystem for estimating g_1 changes between the qubit and the light depending on the affordable time interval as well as the strength of the coupling, in particular g_1. For estimating g_2, in most of the cases, the light is the optimal subsystem. Only when the affordable time interval is short, and g_2 is very small, the optimal subsystem becomes the mechanical oscillator.

V. MULTIPARAMETER ESTIMATION

In this section, we present two different multiparameter estimations scenarios: (i) Estimating only one g_i by assuming the nuisance presence of the other, the so-called nuisance estimation, and (ii) inferring both unknown parameters g_1 and g_2 simultaneously, the so-called joint estimation.

Let us first focus on the nuisance estimation of the parameters g_1 (g_2) in the presence of g_2 (g_1). To do so, we recall from the bounds in Eq. (11) that the expression that quantifies this are the diagonal elements of the inverse of the QFI matrix

$$(\mathcal{Q}^{-1})_{11} := \frac{\mathcal{Q}_{22}}{\mathcal{Q}_{11}\mathcal{Q}_{22} - \mathcal{Q}_{12}^2}, \tag{27}$$

$$(\mathcal{Q}^{-1})_{22} := \frac{\mathcal{Q}_{11}}{\mathcal{Q}_{11}\mathcal{Q}_{22} - \mathcal{Q}_{12}^2}. \tag{28}$$

In Fig. 5, we present the precision limits quantified by $(\mathcal{Q}^{-1})_{ii}$ for the estimation of g_i when the other nuisance parameter g_j is present in the system. Notably, as the figure shows, the nuisance scenario highly resembles the single-parameter estimation case already discussed and shown in Fig. 3. Hence one concludes similar remarks, namely, (i) that the mechanical oscillator (which can only encode g_1 using the cavity field as mediator) poorly performs for the estimation of g_1 [see Figs. 5(a)–5(d)], (ii) analogously the qubit system (which can only encode g_2 through the light field) poorly performs for the estimation of g_2 [see Figs. 5(e)–5(h)], and (iii) having partial accessibility to the qubit or the light parties gives excellent performances, even almost saturating the ultimate global bound. It is worth emphasizing that while the above results share similar conclusions with the single-parameter scenario, they are far from being trivial. The fact that this is the case for the present model shows the relevance of determining the precision limits for each subsystem.

To evidence that the estimation in the presence of nuisance parameters, which employs the multiparameter mathematical tools for its description, would still degrade the estimation of g_i in the presence of an unknown g_j, we define its corresponding nuisance-estimation efficiency ratio as

$$\eta_i^{(\mathrm{multi})} = \left.\frac{(\mathcal{Q}^{-1})_{ii,\mathrm{global}}}{(\mathcal{Q}^{-1})_{ii,\mathrm{sub}}}\right|_{t=t^*}, \tag{29}$$

where t^* is the time where the optimal subsystem reaches its minimum within a given time interval. In Fig. 6 we illustrate the efficiency for this scenario. As seen from the figure, even in the presence of an unknown parameter, having partial accessibility to the qubit and light subsystem still shows

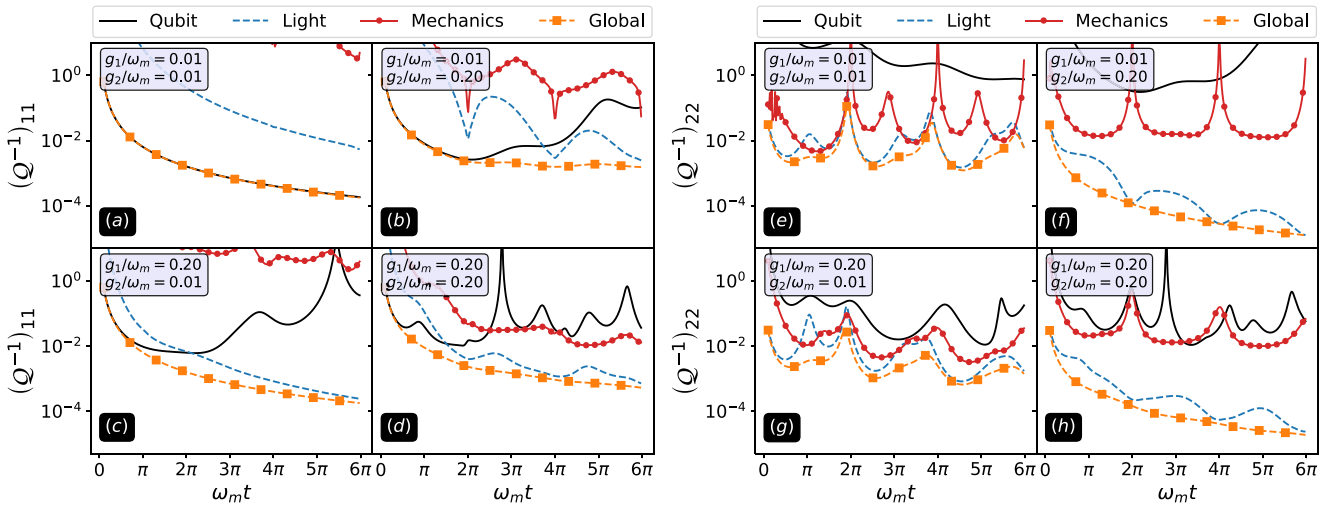

FIG. 5. Precision limits quantified by $(\mathcal{Q}^{-1})_{ii}$ for the estimation of g_i when a nuisance parameter g_j is present in the system.

adequate performance. In particular, in panels (a) and (c) of Fig. 6 one recovers the qubit-to-light efficiency transition shown in Fig. 4 for a similar set of parameters g_1 and g_2. In Figs. 6(b) and 6(d), it is evident that the light field performs better for both time windows with minor degrading when it is compared with the single-parameter scenario in Fig. 4. One concludes that for the present hybrid model, the extra nuisance parameter adds a feeble noise in the final precision limits for this particular multiparameter estimation scenario.

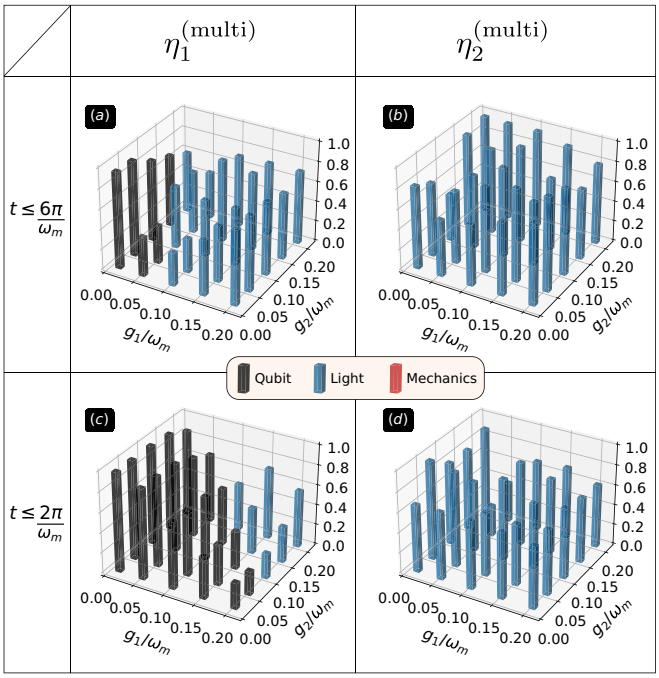

FIG. 6. Panels (a) and (c) show the efficiency for the estimation of g_1 in the presence of a nuisance unknown parameter g_2 for two time intervals. Similarly, panels (b) and (d) show the estimation of g_2 in the presence of a nuisance parameter g_1 for the same time windows.

We now focus on setting the precision limits when both parameters are unknown, the so-called joint estimation. In particular we will consider as our figure of merit the scalar bound in Eq. (10) that in our scenario can be written explicitly as (in the following we omit the number of repetitions for the experiment M)

$$\mathrm{Var}[g_1] + \mathrm{Var}[g_2] \geqslant \mathrm{Tr}[\mathcal{Q}^{-1}] := \frac{\mathcal{Q}_{11} + \mathcal{Q}_{22}}{\mathcal{Q}_{11}\mathcal{Q}_{22} - \mathcal{Q}_{12}^2}, \qquad (30)$$

where $\mathrm{Var}[g_i]$ is the variance for the parameter g_i. The above equations determine the uncertainty in estimating jointly the unknown parameters g_1 and g_2.

In Fig. 7 we plot the joint uncertainty, quantified by $\mathrm{Tr}[\mathcal{Q}^{-1}]$, for the simultaneous estimation of g_1 and g_2. The figure shows that both the qubit and the mechanical parties give poor performances compared with previous estimation scenarios. This can be explained by separating the joint estimation expression into its nuisances elements, i.e., $\mathrm{Tr}[\mathcal{Q}^{-1}] = (\mathcal{Q}^{-1})_{11} + (\mathcal{Q}^{-1})_{22}$. As discussed in Fig. 5, while the qubit (mechanics) provides a good performance in estimating g_1 (g_2), it fails in performing efficiently for the coupling parameter g_2 (g_1). Consequently, the overall additive operation results in estimating both coupling parameters jointly with deficient performances. The above bad additive compensation undermines the qubit and the mechanical oscillator as good probes when the system's parameters are estimated jointly. On the other hand, as evident from Fig. 7 the light subsystem performs exceptionally well within the considered time window remarkably even almost approaching the ultimate precision limits given by accessing the system globally.

As we have mentioned in Sec. II, the multiparameter scalar quantum Cramér-Rao bound is not in general achievable. For this reason we will here also analyze the performance of a particular measurement strategy in order to derive the corresponding classical Fisher information matrix $\mathcal{F}$ and the corresponding multiparameter scalar bound. Previous sections have studied the bounds in estimating g_1 and g_2 in a hybrid nonlinear system with partial accessibility. In particular, our results show that the information content in the

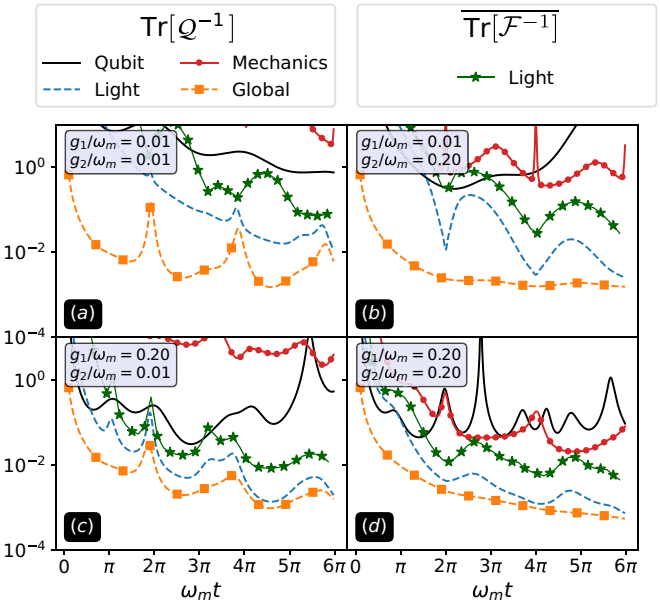

FIG. 7. Precision limits for the joint estimation $\mathrm{Tr}[\mathcal{Q}^{-1}]$ of parameters g_1 and g_2 as a function of time $\omega_m t$ for four coupling parameters. We have also included the optimized classical Fisher information scalar bound, $\overline{\mathrm{Tr}[\mathcal{F}^{-1}]}$, when the light field is measured using a homodyne detection scheme.

cavity field makes it the most suitable subsystem to probe the coupling parameters jointly (see Fig. 7). Therefore we will only present a feasible measurement of the light field for the simultaneous estimation of g_1 and g_2, the widely used homodyne detection [111]. As presented in Sec. II, the scalar bound that quantifies the precision limits in estimating g_1 and g_2 simultaneously for a fixed measurement basis is

$$\mathrm{Var}[g_1] + \mathrm{Var}[g_2] \geqslant \mathrm{Tr}[\mathcal{F}^{-1}], \tag{31}$$

where the equality is reached for an optimal estimator and $\mathcal{F}$ is the classical Fisher information whose elements can be evaluated via Eq. (8) and by considering the homodyne conditional probability $p(x_{\Phi_{\mathrm{LO}}}|\boldsymbol{g})$. In particular we can compute this probability as follows:

$$p(x_{\Phi_{\mathrm{LO}}}|\boldsymbol{g}) = \mathrm{Tr}[|x_{\Phi_{\mathrm{LO}}}\rangle\langle x_{\Phi_{\mathrm{LO}}}|\rho_{\mathrm{light}}(t)], \tag{32}$$

where $|x_{\Phi_{\mathrm{LO}}}\rangle$ is the eigenvector of the rotated quadrature operator x_ϕ with local oscillator phase ϕ defined as

$$x_{\Phi_{\mathrm{LO}}} = \frac{a e^{-i\Phi_{\mathrm{LO}}} + a^\dagger e^{i\Phi_{\mathrm{LO}}}}{\sqrt{2}}, \tag{33}$$

and $\rho_{\mathrm{light}}(t)$ is the reduced density matrix of the light field. Notice that the performance of the homodyne detection depends on the choice of the local phase Φ_{LO}. However, this phase is known and tunable in real experiments and, therefore, we optimize the homodyne detection procedure over Φ_{LO} as

$$\overline{\mathrm{Tr}[\mathcal{F}^{-1}]} := \min_{-\pi \leqslant \Phi_{\mathrm{LO}} \leqslant +\pi} \mathrm{Tr}[\mathcal{F}^{-1}]. \tag{34}$$

In Fig. 7, we contrast the classical Fisher information bound $\overline{\mathrm{Tr}[\mathcal{F}^{-1}]}$ with the quantum bound $\mathrm{Tr}[\mathcal{Q}^{-1}]$. As seen from the figure, the homodyne detection for the light field performs adequately within the time window. Interestingly, despite the fact that the simple optimized homodyne detection is not the optimal measurement basis (which could be unfeasible in practice), its performance is not very far from the optimal one. This shows that one can jointly determine g_1 and g_2 over a wide range merely by performing the homodyne detection on the cavity field.

VI. OPTIMAL SUBSYSTEM IN THE PRESENCE OF IMPERFECTIONS

This section presents the performance of the subsystems for the estimation of g_1 and g_2 in the presence of imperfections. For our purpose, we will restrict the analysis only to imperfections arising from the dynamics while keeping the whole measurement procedure with perfect efficiency. As known, any physical system interacts unavoidably with one or more reservoirs, an inaccessible system with larger degrees of freedom than the system of interest that generally causes detrimental effects to the system's dynamics. From a practical perspective, investigating the system under such detrimental effects is of utmost importance as it determines its feasibility in a more real experimental scenario. To have a fair comparison between the unitary and the nonunitary dynamics, we consider our system to evolve from

$$\rho(0) = |g\rangle\langle g| \otimes |\alpha\rangle\langle\alpha| \otimes \sum_{n=0}^{\infty} \frac{\bar{n}^n}{(1+\bar{n})^{n+1}} |n\rangle\langle n|. \tag{35}$$

As seen from the above, while both the qubit and the cavity are initialized in experimentally available pure states, we have left the mechanical party to evolve from a thermal mixed state in Fock basis with phonon number occupancy $\bar{n}$. In particular, we consider the initial state of the qubit as its ground-state $|g\rangle$, the cavity field with coherent amplitude $\alpha = 2$, and the mechanical oscillator with phonon mean value $\bar{n} = 1$ [26,27].

To model the open (nonunitary) quantum dynamics, we solve the Born-Markov master equation

$$\frac{d\rho}{dt} = -i[H,\rho] + \frac{\kappa}{2}\mathcal{D}[a]\rho + \frac{\gamma_D}{4}\mathcal{D}[\sigma_z]\rho + \gamma\mathcal{D}[\sigma^-]\rho \times \frac{\Gamma}{2}(1+\bar{N})\mathcal{D}[b]\rho + \frac{\Gamma}{2}\bar{N}\mathcal{D}[b^\dagger]\rho, \tag{36}$$

where

$$\mathcal{D}[O]\rho = 2O\rho O^\dagger - \rho O^\dagger O - O^\dagger O\rho, \tag{37}$$

and $\kappa, \Gamma, \gamma_D, \gamma$ account for the cavity intensity decay rate, the mechanical damping rate, the pure dephasing rate, and the qubit relaxation rate, respectively. In Eq. (36), $\bar{N}$ is the average phonon number in thermal equilibrium $\bar{N} = (e^{\omega_m/k_B T} - 1)^{-1}$, where the Planck constant has been set to $\hbar = 1$, T is the temperature of the reservoir, and k_B is the Boltzmann constant. Due to the large difference between the mechanical and the cavity modes, i.e., $\omega_m \ll \omega_c$, we have omitted the average photon number in thermal equilibrium. In what follows, we consider the hybrid system to evolve under the rates $\kappa = 10^{-2}\omega_m$, $\Gamma = 10^{-4}\omega_m$, $\gamma_D = 10^{-2}\omega_m$, and $\gamma = 10^{-2}\omega_m$ embedded in a reservoir with $\bar{N} = 10$ phonon excitations on average.

We first focus on quantifying how much information content is lost when the optimal subsystem decoheres, whereas

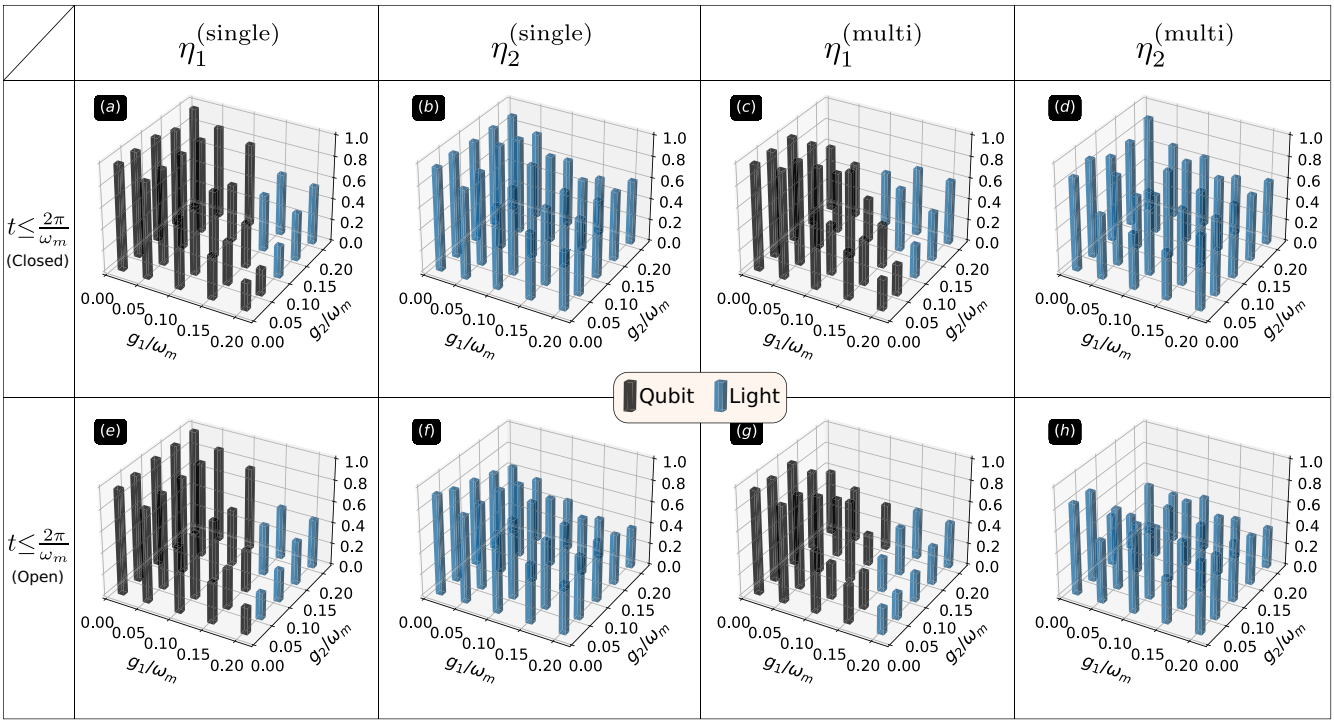

FIG. 8. Panels (a) to (d) show the efficiency ratios for the single-parameter and nuisance multiparameter cases when the optimal subsystem and the global state are computed from a lossless closed dynamics. Panels (e) to (h) show the same as above when the optimal subsystem decoheres while the global state remains lossless.

the global bound remains lossless. To do so, we consider the same efficiency ratios as defined in previous sections, namely, for the single-parameter estimation case

$$\eta_i^{(\mathrm{single})} = \left. \frac{(\mathcal{Q}_{ii})^{-1}_{\mathrm{global,closed}}}{(\mathcal{Q}_{ii})^{-1}_{\mathrm{sub}}} \right|_{t=t^*}, \tag{38}$$

and

$$\eta_i^{(\mathrm{multi})} = \left. \frac{(\mathcal{Q}^{-1})_{ii,\mathrm{global,closed}}}{(\mathcal{Q}^{-1})_{ii,\mathrm{sub}}} \right|_{t=t^*}, \tag{39}$$

for the nuisance multiparameter estimation scenario. Notice that we have stressed in the above numerators that the global state evolves as a closed (lossless) system, while the optimal subsystem will undergo closed or open dynamics.

In Figs. 8(a)–8(d), we show the efficiency ratios for the single-parameter and nuisance multiparameter cases when the optimal subsystem and the global state are computed from a unitary dynamics. Notice that with the choice of a more experimental mechanical state initialization with $\bar{n} \lesssim 1$ [26,27], one reaches similar conclusions as to when the system evolves from a coherent mechanical oscillator. In particular, from Figs. 8(a)–8(d), it is evident that for estimating g_1 the optimal subsystems can be either the qubit or the cavity field depending on the set of g_1 and g_2 parameters. Moreover, very high performances can be reached especially for weak values of g_1. Additionally, for the estimation of g_2, the cavity field is the dominant optimal subsystem for all the considered ranges of g_1 and g_2 parameters. In Figs. 8(e)–8(h), we show the efficiency ratios for the single-parameter and nuisance multiparameter cases when the optimal subsystem decoheres and the global state remains to evolve without losses. Interestingly, as seen from the figures, the efficiency ratios are mildly attenuated. In other words, for the set of lossy parameters considered here, one can argue that not much information content is lost within that time interval, making the single-parameter and the nuisance multiparameter estimation robust under decoherence.

We now turn attention to quantify how much information content the global state loses in the presence of decoherence. To do so, let us define the single-parameter efficiency ratio between global states as

$$\mu_i^{(\mathrm{single})} = \left. \frac{(\mathcal{Q}_{ii})^{-1}_{\mathrm{global,closed}}}{(\mathcal{Q}_{ii})^{-1}_{\mathrm{global,open}}} \right|_{t=t^*}, \tag{40}$$

and

$$\mu_i^{(\mathrm{multi})} = \left. \frac{(\mathcal{Q}^{-1})_{ii,\mathrm{global,closed}}}{(\mathcal{Q}^{-1})_{ii,\mathrm{global,open}}} \right|_{t=t^*} \tag{41}$$

being the nuisance multiparameter efficiency ratio between global states undergoing a closed and an open evolution.

In Figs. 9(a)–9(d), we plot the single-parameter efficiency ratio between global states as well as the nuisance multiparameter efficiency ratio between global states. As seen from the figures, the attenuation of the information content in the whole state is around $\sim$20% for the set of damping ratios considered for the numerical simulations. One can conclude that both the optimal subsystems as well as the global bounds in the presence of imperfections still have enough information for the estimation of the g_1 and g_2 parameters.

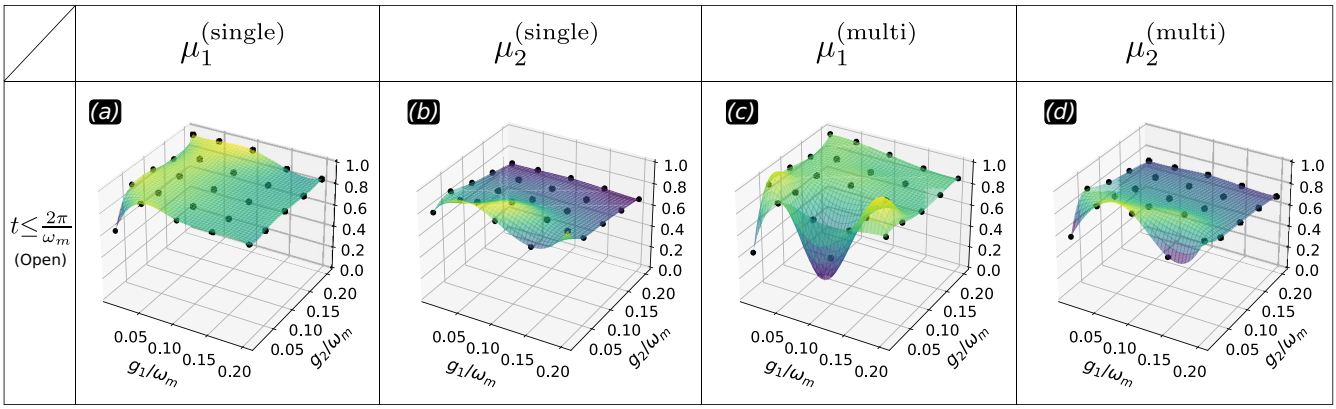

FIG. 9. Panels (a) and (b) show the single-parameter efficiency ratio between closed and open global states. Panels (c) and (d) show the nuisance multiparameter efficiency ratio between global states.

VII. EXPERIMENTAL FEASIBILITY

Recent experimental efforts to hybridize electro- or optomechanical systems with a nonlinear constituent, such as a qubit, have been developed in devices including gigahertz superconducting circuits with Cooper pair boxes as qubits [67], trapped Rubidium atoms in photonic crystal cavities [112,113], trapped ions $^{40}Ca^{+}$-ions in fiber cavities [112,114], defect centers in silica toroids [115], and gallium-arsenide optomechanical resonators with cavity QED couplings [116,117], among others. The inclusion of a qubit, coupled either to the cavity or to the mechanical modes, allows us to operate in the somewhat elusive optomechanical regime, namely, the strong single-photon radiation pressure interaction ($g_2 \gtrsim \kappa$) [118] and the resolved sideband condition ($\kappa < \omega_m$) simultaneously. Consequently, throughout our work, we consider $g_1 \in (0, 0.2\omega_m]$, $g_2 \in (0, 0.2\omega_m]$, the resonant qubit-cavity case $\omega_q = \omega_c$, $\omega_c = 100\omega_m$, $\kappa = 10^{-2}\omega_m$, $\Gamma = 10^{-4}\omega_m$, $\gamma_D = 10^{-2}\omega_m$, $\gamma = 10^{-2}\omega_m$, and $\bar{N} = 10$, a set of parameters that can already be achieved in electromechanical systems in the microwave regime. In particular, in order to justify our set of parameters, we will focus on Ref. [67] where for the first time a hybrid qubit-electromechanical system was fully integrated and characterized. There a large d.c. voltage bias between 5 to 10 V applied to the mechanical degree of freedom couples via a movable capacitance to the charge qubit composed of Josephson tunnel junctions. In this case, the obtained hybrid characterization values carried out in a dilution refrigerator at 20 mK temperature are $\omega_c/2\pi = 4.93$ GHz, $\omega_m/2\pi \simeq 65$ MHz of the lowest flexural mode, and g_1/ω_m ranges up to scaled coupling qubit-cavity QED frequencies of 10 MHz (i.e., $g_1/\omega_c \sim 1$ near the deep-strong coupling regime). Remarkably, in the absence of the qubit, an estimation of the bare electromechanical coupling gives $g_2/\omega_m \sim 0.15 \times 10^{-7}$, while by switching on the qubit coupling, the bare electromechanical coupling increases up to six orders of magnitude $g_2/\omega_m \sim 0.25 \times 10^{-1}$ and claimed in the same Ref. [67] that an exceeding boosting of the electromechanical radiation pressure up to eight orders of magnitude could be achieved through an optimized device giving rise to $g_2 \sim \omega_m$. The decoherence parameters are $\Gamma \lesssim 10^{-5}\omega_m$, with $\bar{N} \sim 6$, $\gamma \sim \omega_m$ and $0.025 \lesssim \kappa/\omega_m \lesssim 0.1$. The above justifies the parameters considered throughout our work within state-of-the-art experiments or near-future developments toward this hybrid route.

VIII. CONCLUDING REMARKS

In this paper, we investigate the possibility of dynamically estimating the couplings between qubit-light and light-mechanics in a hybrid optomechanical system. Although the quantum state of the entire system carries a wealth of information about the couplings, in practice extracting such information demands global measurements which are not readily available. Thus the most sensible approach is to estimate the couplings through measurements on one of the subsystems, namely, the qubit, cavity light, or the mechanical oscillator. Due to the entanglement between different components of the system, the reduced density matrix of each subsystem is mixed, and thus it is not obvious how much information one can extract via this partial accessibility. We show that indeed the couplings can be estimated through partial accessibility with the precision not very far from the global bound. Our comprehensive analysis shows that for estimating the light-mechanics coupling, the light field is dominantly the optimal subsystem to be measured. Interestingly, this is also the case for simultaneous joint estimation of the two couplings. On the other hand, for estimating the qubit-light coupling, depending on the situation either the qubit or the light field can be the optimal subsystems. For instance, in the case of single-parameter and nuisance multiparameter estimation, depending on the range of the qubit-light coupling, the optimal subsystem can change from the qubit to the cavity field. The reason that light is the most suitable subsystem for inferring the couplings is that the light is responsible for mediating the interaction between the other two parties. Finally, for the sake of completeness, we show that a simple widely used homodyne measurement on the light degrees of freedom can extract the values of the couplings with a fair precision.

ACKNOWLEDGMENTS

A.B. acknowledges support from the National Key R&D Program of China for Grant No. 2018YFA0306703, the National Science Foundation of China for Grants No.

12050410253 and No. 92065115, and the Ministry of Science and Technology of China for the Young Scholars National Foreign Expert Project for Grant No. QNJ2021167001L. V.M. thanks the National Natural Science Foundation of China for Grant No. 12050410251, the Chinese Postdoctoral Science Fund for Grant No. 2018M643435, and the Ministry of Science and Technology of China for the Young Scholars National Foreign Expert Project for Grant No. QNJ2021167004. M.G.G. acknowledges support from UniMi-PSR-2020 and UniMi-PSR-2021 projects.

APPENDIX: JC-LIKE DYNAMICS

This section puts forward key aspects of the tripartite system which will help us understand the role of the mechanical displacement in JC dynamics. Indeed, several works have already considered such hybrid Hamiltonian in Eq. (13). In particular, within the single-photon subspace, it has been studied in the regimes where $g_1 \ll \omega_m$, g_2 and $g_2 \approx \omega_m$ leading to slow Rabi oscillations and the case $g_2 \ll \omega_m$ where they are almost suppressed [119]. Additionally, lifting the single-photon subspace restriction has shown that the population inversion exhibits anomalous oscillations induced by the mechanical displacement for $g_2 \ll \omega_m$ and different initial states for the light field and the mechanical object [120]. For the sake of completeness, we briefly present and discuss the derivation of the JC-like Hamiltonian derived in Refs. [64,103], where the mechanical displacement explicitly couples to a qubit-light polariton doublet.

Let us first consider the polariton-phonon basis $\{|\pm^{(n)}, m\rangle\}$ for the resonant case ($\omega_q = \omega_c$), where m is an integer and $|\pm^{(n)}\rangle$ are the polariton JC dressed states defined as ($n = 0$ returns $|g, 0\rangle$)

$$\forall n \in \mathbb{N}, n \neq 0,$$
$$\left|+^{(n)}\right\rangle = \frac{1}{\sqrt{2}}(|g, n\rangle + |e, n-1\rangle), \tag{A1}$$
$$\left|-^{(n)}\right\rangle = \frac{1}{\sqrt{2}}(|g, n\rangle - |e, n-1\rangle). \tag{A2}$$

As known, the polariton basis exactly diagonalizes the JC Hamiltonian (i.e., $g_2 = 0$), and hence the basis $\{|\pm^{(n)}, m\rangle\}$ enables us to write the hybrid Hamiltonian in Eq. (13) as follows:

$$H = \omega_m b^\dagger b + \sum_{n\in\mathbb{N}} H^{(n)},$$
$$H^{(n)} = \left(n - \frac{1}{2}\right)\omega_c \mathbb{I}^{(n)} + \frac{\Omega^{(n)}}{2}\sigma_z^{(n)} - g_2\left\{\frac{1}{2}\sigma_x^{(n)} + \left(n - \frac{1}{2}\right)\mathbb{I}^{(n)}(b + b^\dagger)\right\}, \tag{A3}$$

where $\Omega^{(n)} = 2\sqrt{n}g_1$, $\mathbb{I}^{(n)}$ is the identity matrix in the subspace spanned by the set $\{|+^{(n)}\rangle, |-^{(n)}\rangle\}$, and $\sigma_i^{(n)}$ are Pauli matrices acting on the same polariton subspace. Two readily evident features can be drawn from Eq. (A3), namely, (i) each of the two cavity polariton states $\{|\pm^{(n)}, m\rangle\}$ couples effectively to the mechanical's position evidenced by $\propto \sigma_x^{(n)}(b + b^\dagger)$, and (ii) each $\{|\pm^{(n)}, m\rangle\}$ contains on average $n-1/2$ excitations that displace the equilibrium position of the mechanical object. One can further absorb the latter n-dependent mechanical equilibrium displacement by introducing

$$b = b_n + \frac{g_2}{\omega_m}\left(n - \frac{1}{2}\right). \tag{A4}$$

The above new operator b_n introduces an associated Fock basis $|m^{(n)}\rangle$, with $m^{(n)} \in \mathbb{N}$ phonons for the mechanical mode centered at $\sqrt{2}g_2/\omega_m(n - 1/2)$. The above transformation leads to the effective JC-like Hamiltonian for the weak single-photon optomechanical regime $g_2 \ll \omega_m$ [64],

$$H \simeq \sum_{n\in\mathbb{N}} \omega_m b_n^\dagger b_n + \sqrt{n}g_1\sigma_z^{(n)} - \frac{g_2}{2}\left(b_n^\dagger\sigma_-^{(n)} + b_n\sigma_+^{(n)}\right). \tag{A5}$$

It is worth emphasizing that in the above we have performed the rotating wave approximation for each n polariton subspace, namely, $|\omega_m - \Omega^{(n)}| \ll \omega_m + \Omega^{(n)}$.

Since the polariton number operator $N = a^\dagger a + \sigma_+\sigma_-$ permits us to diagonalize the JC Hamiltonian in the basis $\{|\pm^{(n)}, m\rangle\}$, one can employ the same techniques to diagonalize the Hamiltonian in Eq. (A5) by defining a polaron number operator as

$$N_{\text{polaron}} = b_n^\dagger b_n + \sigma_+^{(n)}\sigma_-^{(n)}. \tag{A6}$$

This readily lead us to the polaron eigenbasis

$$\Omega^{(n)} \neq \omega_m,$$
$$\begin{pmatrix} \left|+^{n,m^{(n)}}\right\rangle \\ \left|-^{n,m^{(n)}}\right\rangle \end{pmatrix} = R(2\theta^{n,m^{(n)}})\begin{pmatrix} \left|+^{(n)}\right\rangle\left|(m-1)^{n,m^{(n)}}\right\rangle \\ \left|-^{(n)}\right\rangle\left|m^{n,m^{(n)}}\right\rangle \end{pmatrix}, \tag{A7}$$

where

$$R\left(2\theta^{n,m^{(n)}}\right) = \begin{pmatrix} \cos\theta^{n,m^{(n)}} & \sin\theta^{n,m^{(n)}} \\ \sin\theta^{n,m^{(n)}} & -\cos\theta^{n,m^{(n)}} \end{pmatrix}, \tag{A8}$$

such that

$$\theta^{n,m^{(n)}} \in \left(-\frac{\pi}{2}, 0\right],$$
$$\tan 2\theta^{n,m^{(n)}} = \frac{g_2\sqrt{m^{(n)}}}{\sqrt{\left(\Omega^{(n)} - \omega_m\right)^2 + g_2^2 m^{(n)}}}, \tag{A9}$$

and associated polaron eigenenergies

$$E_\pm^{n,m^{(n)}} = \pm\sqrt{\frac{(\Omega^{(n)} - \omega_m)^2}{4} + m^{(n)}\frac{g_2^2}{4}} + \omega_0^{(n)} + \left(m^{(n)} - \frac{1}{2}\right)\omega_m. \tag{A10}$$

While the unitary dynamics can be now solved straightforward using

$$|\psi(t)\rangle = \sum_{\substack{n=0 \\ m^{(n)}=0}}^{\infty} \sum_{j=+,-} e^{-itE_j^{n,m^{(n)}}}\left|j^{n,m^{(n)}}\right\rangle\left\langle j^{n,m^{(n)}}\right|\psi(0)\rangle, \tag{A11}$$

special attention must be paid for the inner product between the Fock states of b and the displaced basis b_n which obeys

$$\forall m^{(n)}, l \in \mathbb{N},$$
$$\left\langle l|m^{(n)}\right\rangle = L_{m^{(n)}}^{l-m^{(n)}}\left(\left[\frac{g_2}{\omega_m}\left(n - \frac{1}{2}\right)\right]^2\right)e^{-\left[\frac{g_2}{\omega_m}\left(n-\frac{1}{2}\right)\right]^2} \times\sqrt{\frac{m^{(n)}!}{l!}}\left[\frac{g_2}{\omega_m}\left(n - \frac{1}{2}\right)\right]^{l-m^{(n)}}, \tag{A12}$$

where $L_{m^{(n)}}^{l-m^{(n)}}(x)$ is the generalized Laguerre polynomial of degree $m^{(n)}$ and index $l - m^{(n)}$.

The above brief review on the diagonalization of the hybrid tripartite Hamiltonian in polaron basis serves two main purposes, namely, (i) the effective JC-like Hamiltonian neglects a Star-like shift in the eigenenergies induced by $\sigma_x^{(n)} g_2^2 (n - 1/2)/\omega_m$, which must be taken into account when the single-photon coupling enters the strong-to-moderate optomechanical regime, and (ii) the polaron picture shows that the mechanical oscillator couples independently to each polariton doublet. Similar effective Hamiltonians have been also derived by different techniques, for instance, by a displaced transformation picture [120,121] and through an operator approach [122].

[1] S. Haroche and J. M. Raimond, *Exploring the Quantum: Atoms, Cavities, and Photons* (Oxford University Press, Oxford, 2006).

[2] H. Walther, B. T. H. Varcoe, B.-G. Englert, and T. Becker, Cavity quantum electrodynamics, Rep. Prog. Phys. **69**, 1325 (2006).

[3] H. Mabuchi and A. C. Doherty, Cavity quantum electrodynamics: Coherence in context, Science **298**, 1372 (2002).

[4] D. Meschede, H. Walther, and G. Müller, One-Atom Maser, Phys. Rev. Lett. **54**, 551 (1985).

[5] K. An, J. J. Childs, R. R. Dasari, and M. S. Feld, Microlaser: A laser with One Atom in an Optical Resonator, Phys. Rev. Lett. **73**, 3375 (1994).

[6] A. Reiserer, N. Kalb, G. Rempe, and S. Ritter, A quantum gate between a flying optical photon and a single trapped atom, Nature (London) **508**, 237 (2014).

[7] B. Hacker, S. Welte, G. Rempe, and S. Ritter, A photon–photon quantum gate based on a single atom in an optical resonator, Nature (London) **536**, 193 (2016).

[8] C. J. Hood, T. W. Lynn, A. C. Doherty, A. S. Parkins, and H. J. Kimble, The atom-cavity microscope: Single atoms bound in orbit by single photons, Science **287**, 1447 (2000).

[9] P. W. H. Pinkse, T. Fischer, P. Maunz, and G. Rempe, Trapping an atom with single photons, Nature (London) **404**, 365 (2000).

[10] A. Blais, R.-S. Huang, A. Wallraff, S. M. Girvin, and R. J. Schoelkopf, Cavity quantum electrodynamics for superconducting electrical circuits: An architecture for quantum computation, Phys. Rev. A **69**, 062320 (2004).

[11] S. Haroche, Quantum information in cavity quantum electrodynamics: Logical gates, entanglement engineering and 'schrödinger-cat states', Philos. Trans.: Math., Phys. Eng. Sci. **361**, 1339 (2003).

[12] A. D. Greentree, J. Koch, and J. Larson, Fifty years of jaynes–cummings physics, J. Phys. B: At., Mol. Opt. Phys. **46**, 220201 (2013).

[13] B. W. Shore and P. L. Knight, The Jaynes-Cummings model, J. Mod. Opt. **40**, 1195 (1993).

[14] M. Tavis and F. W. Cummings, Exact solution for an *n*-molecule—radiation-field Hamiltonian, Phys. Rev. **170**, 379 (1968).

[15] M. Tavis and F. W. Cummings, Approximate solutions for an *n*-molecule-radiation-field Hamiltonian, Phys. Rev. **188**, 692 (1969).

[16] D. G. Angelakis, M. F. Santos, and S. Bose, Photon-blockade-induced mott transitions and *xy* spin models in coupled cavity arrays, Phys. Rev. A **76**, 031805(R) (2007).

[17] A. D. Greentree, C. Tahan, J. H. Cole, and L. C. L. Hollenberg, Quantum phase transitions of light, Nat. Phys. **2**, 856 (2006).

[18] M. J. Hartmann, F. G. S. L. Brandão, and M. B. Plenio, Strongly interacting polaritons in coupled arrays of cavities, Nat. Phys. **2**, 849 (2006).

[19] M. Aspelmeyer, T. J. Kippenberg, and F. Marquardt, Cavity optomechanics, Rev. Mod. Phys. **86**, 1391 (2014).

[20] H. Xiong, L. Si, X. Lv, X. Yang, and Y. Wu, Review of cavity optomechanics in the weak-coupling regime: From linearization to intrinsic nonlinear interactions, Sci. China: Phys., Mech. Astron. **58**, 1 (2015).

[21] Yu-long Liu, C. Wang, J. Zhang, and Yu-xi Liu, Cavity optomechanics: Manipulating photons and phonons towards the single-photon strong coupling, Chin. Phys. B **27**, 024204 (2018).

[22] C. K. Law, Interaction between a moving mirror and radiation pressure: A Hamiltonian formulation, Phys. Rev. A **51**, 2537 (1995).

[23] S. Qvarfort, A. Serafini, A. Xuereb, D. Braun, D. Rätzel, and D. E. Bruschi, Time-evolution of nonlinear optomechanical systems: Interplay of mechanical squeezing and non-gaussianity, J. Phys. A: Math. Theor. **53**, 075304 (2020).

[24] S. Bose, K. Jacobs, and P. L. Knight, Preparation of nonclassical states in cavities with a moving mirror, Phys. Rev. A **56**, 4175 (1997).

[25] S. Mancini, V. I. Man'ko, and P. Tombesi, Ponderomotive control of quantum macroscopic coherence, Phys. Rev. A **55**, 3042 (1997).

[26] A. D. O'Connell, M. Hofheinz, M. Ansmann, R. C. Bialczak, M. Lenander, E. Lucero, M. Neeley, D. Sank, H. Wang, M. Weides, J. Wenner, J. M. Martinis, and A. N. Cleland, Quantum ground state and single-phonon control of a mechanical resonator, Nature (London) **464**, 697 (2010).

[27] J. Chan, T. P. M. Alegre, A. H. Safavi-Naeini, J. T. Hill, A. Krause, S. Gröblacher, M. Aspelmeyer, and O. Painter, Laser cooling of a nanomechanical oscillator into its quantum ground state, Nature (London) **478**, 89 (2011).

[28] A. C. Doherty, A. Szorkovszky, G. I. Harris, and W. P. Bowen, The quantum trajectory approach to quantum feedback control of an oscillator revisited, Philos. Trans. R. Soc. A **370**, 5338 (2012).

[29] N. T. Otterstrom, R. O. Behunin, E. A. Kittlaus, and P. T. Rakich, Optomechanical Cooling in a Continuous System, Phys. Rev. X **8**, 041034 (2018).

[30] Y.-C. Liu, Y.-W. Hu, C. W. Wong, and Y.-F. Xiao, Review of cavity optomechanical cooling, Chin. Phys. B **22**, 114213 (2013).

[31] R. Rivière, S. Deléglise, S. Weis, E. Gavartin, O. Arcizet, A. Schliesser, and T. J. Kippenberg, Optomechanical sideband cooling of a micromechanical oscillator close to the quantum ground state, Phys. Rev. A **83**, 063835 (2011).

[32] D. Kleckner and D. Bouwmeester, Sub-kelvin optical cooling of a micromechanical resonator, Nature (London) **444**, 75 (2006).

[33] M. R. Vanner, J. Hofer, G. D. Cole, and M. Aspelmeyer, Cooling-by-measurement and mechanical state tomography via pulsed optomechanics, Nat. Commun. **4**, 2295 (2013).

[34] A. Schliesser, P. Del'Haye, N. Nooshi, K. J. Vahala, and T. J. Kippenberg, Radiation Pressure Cooling of a Micromechanical Oscillator Using Dynamical Backaction, Phys. Rev. Lett. **97**, 243905 (2006).

[35] I. Wilson-Rae, P. Zoller, and A. Imamoğlu, Laser Cooling of a Nanomechanical Resonator Mode to its Quantum Ground State, Phys. Rev. Lett. **92**, 075507 (2004).

[36] S. Mancini, D. Vitali, and P. Tombesi, Optomechanical Cooling of a Macroscopic Oscillator by Homodyne Feedback, Phys. Rev. Lett. **80**, 688 (1998).

[37] I. Martin, A. Shnirman, L. Tian, and P. Zoller, Ground-state cooling of mechanical resonators, Phys. Rev. B **69**, 125339 (2004).

[38] K. Jaehne, K. Hammerer, and M. Wallquist, Ground-state cooling of a nanomechanical resonator via a Cooper-pair box qubit, New J. Phys. **10**, 095019 (2008).

[39] D. D. Bhaktavatsala Rao, S. A. Momenzadeh, and J. Wrachtrup, Heralded Control of Mechanical Motion by Single Spins, Phys. Rev. Lett. **117**, 077203 (2016).

[40] V. Montenegro, R. Coto, V. Eremeev, and M. Orszag, Ground-state cooling of a nanomechanical oscillator with n spins, Phys. Rev. A **98**, 053837 (2018).

[41] A. Kronwald, F. Marquardt, and A. A. Clerk, Arbitrarily large steady-state bosonic squeezing via dissipation, Phys. Rev. A **88**, 063833 (2013).

[42] E. E. Wollman, C. U. Lei, A. J. Weinstein, J. Suh, A. Kronwald, F. Marquardt, A. A. Clerk, and K. C. Schwab, Quantum squeezing of motion in a mechanical resonator, Science **349**, 952 (2015).

[43] D. J. Wilson, V. Sudhir, N. Piro, R. Schilling, A. Ghadimi, and T. J. Kippenberg, Measurement-based control of a mechanical oscillator at its thermal decoherence rate, Nature (London) **524**, 325 (2015).

[44] J.-M. Pirkkalainen, E. Damskägg, M. Brandt, F. Massel, and M. A. Sillanpää, Squeezing of Quantum Noise of Motion in a Micromechanical Resonator, Phys. Rev. Lett. **115**, 243601 (2015).

[45] M. G. Genoni, M. Bina, S. Olivares, G. D. Chiara, and M. Paternostro, Squeezing of mechanical motion via qubit-assisted control, New J. Phys. **17**, 013034 (2015).

[46] M. G. Genoni, J. Zhang, J. Millen, P. F. Barker, and A. Serafini, Quantum cooling and squeezing of a levitating nanosphere via time-continuous measurements, New J. Phys. **17**, 073019 (2015).

[47] M. Rossi, D. Mason, J. Chen, Y. Tsaturyan, and A. Schliesser, Measurement-based quantum control of mechanical motion, Nature (London) **563**, 53 (2018).

[48] M. Rossi, D. Mason, J. Chen, and A. Schliesser, Observing and Verifying the Quantum Trajectory of a Mechanical Resonator, Phys. Rev. Lett. **123**, 163601 (2019).

[49] L. Magrini, P. Rosenzweig, C. Bach, A. Deutschmann-Olek, S. G. Hofer, S. Hong, N. Kiesel, A. Kugi, and M. Aspelmeyer, Real-time optimal quantum control of mechanical motion at room temperature, Nature (London) **595**, 373 (2021).

[50] F. Tebbenjohanns, M. L. Mattana, M. Rossi, M. Frimmer, and L. Novotny, Quantum control of a nanoparticle optically levitated in cryogenic free space, Nature (London) **595**, 378 (2021).

[51] G. D. de Moraes Neto, F. M. Andrade, V. Montenegro, and S. Bose, Quantum state transfer in optomechanical arrays, Phys. Rev. A **93**, 062339 (2016).

[52] V. Montenegro, A. Ferraro, and S. Bose, Enabling entanglement distillation via optomechanics, Phys. Rev. A **100**, 042310 (2019).

[53] G. D. de Moraes Neto, V. Montenegro, V. F. Teizen, and E. Vernek, Dissipative phonon-fock-state production in strong nonlinear optomechanics, Phys. Rev. A **99**, 043836 (2019).

[54] M. Hosseini, G. Guccione, H. J. Slatyer, B. C. Buchler, and P. K. Lam, Multimode laser cooling and ultra-high sensitivity force sensing with nanowires, Nat. Commun. **5**, 4663 (2014).

[55] O. Arcizet, P.-F. Cohadon, T. Briant, M. Pinard, A. Heidmann, J.-M. Mackowski, C. Michel, L. Pinard, O. Français, and L. Rousseau, High-Sensitivity Optical Monitoring of a Micromechanical Resonator with a Quantum-Limited Optomechanical Sensor, Phys. Rev. Lett. **97**, 133601 (2006).

[56] J. Chaste, A. Eichler, J. Moser, G. Ceballos, R. Rurali, and A. Bachtold, A nanomechanical mass sensor with yoctogram resolution, Nat. Nanotechnol. **7**, 301 (2012).

[57] A. G. Krause, M. Winger, T. D. Blasius, Q. Lin, and O. Painter, A high-resolution microchip optomechanical accelerometer, Nat. Photonics **6**, 768 (2012).

[58] S. Qvarfort, A. Serafini, P. F. Barker, and S. Bose, Gravimetry through non-linear optomechanics, Nat. Commun. **9**, 3690 (2018).

[59] S. Qvarfort, A. D. K. Plato, D. E. Bruschi, F. Schneiter, D. Braun, A. Serafini, and D. Rätzel, Optimal estimation of time-dependent gravitational fields with quantum optomechanical systems, Phys. Rev. Res. **3**, 013159 (2021).

[60] V. Montenegro, M. G. Genoni, A. Bayat, and M. G. A. Paris, Mechanical oscillator thermometry in the nonlinear optomechanical regime, Phys. Rev. Res. **2**, 043338 (2020).

[61] B. Rogers, N. Lo Gullo, G. De Chiara, G. M. Palma, and M. Paternostro, Hybrid optomechanics for quantum technologies, Quantum Measurements and Quantum Metrology **2**, 11 (2014).

[62] G. Kurizki, P. Bertet, Y. Kubo, K. Mølmer, D. Petrosyan, P. Rabl, and J. Schmiedmayer, Quantum technologies with hybrid systems, Proc. Natl. Acad. Sci. U.S.A. **112**, 3866 (2015).

[63] M. Wallquist, K. Hammerer, P. Rabl, M. Lukin, and P. Zoller, Hybrid quantum devices and quantum engineering, Phys. Scr. **2009**, 014001 (2009).

[64] J. Restrepo, C. Ciuti, and I. Favero, Single-Polariton Optomechanics, Phys. Rev. Lett. **112**, 013601 (2014).

[65] J. Restrepo, I. Favero, and C. Ciuti, Fully coupled hybrid cavity optomechanics: Quantum interferences and correlations, Phys. Rev. A **95**, 023832 (2017).

[66] C. Genes, D. Vitali, and P. Tombesi, Emergence of atom-light-mirror entanglement inside an optical cavity, Phys. Rev. A **77**, 050307(R) (2008).

[67] J.-M. Pirkkalainen, S. U. Cho, F. Massel, J. Tuorila, T. T. Heikkilä, P. J. Hakonen, and M. A. Sillanpää, Cavity optomechanics mediated by a quantum two-level system, Nat. Commun. **6**, 6981 (2015).

[68] A. S. Aporvari and D. Vitali, Strong coupling optomechanics mediated by a qubit in the dispersive regime, Entropy **23**, 966 (2021).

[69] A. Carmele, B. Vogell, K. Stannigel, and P. Zoller, Opto-nanomechanics strongly coupled to a Rydberg superatom: coherent versus incoherent dynamics, New J. Phys. **16**, 063042 (2014).

[70] O. Černotík, C. Genes, and A. Dantan, Interference effects in hybrid cavity optomechanics, Quantum Sci. Technol. **4**, 024002 (2019).

[71] C. Genes, H. Ritsch, and D. Vitali, Micromechanical oscillator ground-state cooling via resonant intracavity optical gain or absorption, Phys. Rev. A **80**, 061803(R) (2009).

[72] W. Zeng, W. Nie, L. Li, and A. Chen, Ground-state cooling of a mechanical oscillator in a hybrid optomechanical system including an atomic ensemble, Sci. Rep. **7**, 17258 (2017).

[73] W. Nie, A. Chen, and Y. Lan, Cooling mechanical motion via vacuum effect of an ensemble of quantum emitters, Opt. Express **23**, 30970 (2015).

[74] Ben-yuan Zhou and Gao-xiang Li, Ground-state cooling of a nanomechanical resonator via single-polariton optomechanics in a coupled quantum-dot–cavity system, Phys. Rev. A **94**, 033809 (2016).

[75] K. Stannigel, P. Rabl, A. S. Sørensen, P. Zoller, and M. D. Lukin, Optomechanical Transducers for Long-Distance Quantum Communication, Phys. Rev. Lett. **105**, 220501 (2010).

[76] K. Stannigel, P. Rabl, A. S. Sørensen, M. D. Lukin, and P. Zoller, Optomechanical transducers for quantum-information processing, Phys. Rev. A **84**, 042341 (2011).

[77] K. Stannigel, P. Rabl, and P. Zoller, Driven-dissipative preparation of entangled states in cascaded quantum-optical networks, New J. Phys. **14**, 063014 (2012).

[78] S. J. M. Habraken, K. Stannigel, M. D. Lukin, P. Zoller, and P. Rabl, Continuous mode cooling and phonon routers for phononic quantum networks, New J. Phys. **14**, 115004 (2012).

[79] C. Dong, Y. Wang, and H. Wang, Optomechanical interfaces for hybrid quantum networks, Natl. Sci. Rev. **2**, 510 (2015).

[80] V. Bergholm, W. Wieczorek, T. Schulte-Herbrüggen, and M. Keyl, Optimal control of hybrid optomechanical systems for generating non-classical states of mechanical motion, Quantum Sci. Technol. **4**, 034001 (2019).

[81] H. Wang, X. Gu, Yu-xi Liu, A. Miranowicz, and F. Nori, Tunable photon blockade in a hybrid system consisting of an optomechanical device coupled to a two-level system, Phys. Rev. A **92**, 033806 (2015).

[82] J. Zhang, T. Zhang, A. Xuereb, D. Vitali, and J. Li, More nonlocality with less entanglement in a tripartite atom-optomechanical system, Ann. Phys. **527**, 147 (2015).

[83] Z.-L. Xiang, S. Ashhab, J. Q. You, and F. Nori, Hybrid quantum circuits: Superconducting circuits interacting with other quantum systems, Rev. Mod. Phys. **85**, 623 (2013).

[84] C. W. Helstrom, *Quantum Detection and Estimation Theory* (Academic Press, New York, 1976).

[85] A. S. Holevo, *Probabilistic and Statistical Aspects of Quantum Theory*, 2nd ed. (Edizioni della Normale, Pisa, 2011).

[86] M. G. A. Paris, Quantum estimation for quantum technology, Int. J. Quantum Inform. **07**, 125 (2009).

[87] F. Albarelli, M. Barbieri, M. G. Genoni, and I. Gianani, A perspective on multiparameter quantum metrology: From theoretical tools to applications in quantum imaging, Phys. Lett. A **384**, 126311 (2020).

[88] J. Liu, H. Yuan, X.-M. Lu, and X. Wang, Quantum Fisher information matrix and multiparameter estimation, J. Phys. A: Math. Theor. **53**, 023001 (2020).

[89] H. Yuan and C.-H. Fred Fung, Quantum parameter estimation with general dynamics, npj Quantum Inf. **3**, 14 (2017).

[90] V. Montenegro, U. Mishra, and A. Bayat, Global Sensing and Its Impact for Quantum Many-Body Probes with Criticality, Phys. Rev. Lett. **126**, 200501 (2021).

[91] M. G. Genoni and C. Invernizzi, Optimal quantum estimation of the coupling constant of Jaynes-Cummings interaction, Eur. Phys. J.: Spec. Top. **203**, 49 (2012).

[92] J. Z. Bernád, C. Sanavio, and A. Xuereb, Optimal estimation of matter-field coupling strength in the dipole approximation, Phys. Rev. A **99**, 062106 (2019).

[93] H. Chen and H. Yuan, Optimal joint estimation of multiple rabi frequencies, Phys. Rev. A **99**, 032122 (2019).

[94] L. Latmiral, F. Armata, M. G. Genoni, I. Pikovski, and M. S. Kim, Probing anharmonicity of a quantum oscillator in an optomechanical cavity, Phys. Rev. A **93**, 052306 (2016).

[95] J. Z. Bernád, C. Sanavio, and A. Xuereb, Optimal estimation of the optomechanical coupling strength, Phys. Rev. A **97**, 063821 (2018).

[96] C. Sanavio, J. Z. Bernád, and A. Xuereb, Fisher-information-based estimation of optomechanical coupling strengths, Phys. Rev. A **102**, 013508 (2020).

[97] K. Sala, T. Doicin, A. D. Armour, and T. Tufarelli, Quantum estimation of coupling strengths in driven-dissipative optomechanics, Phys. Rev. A **104**, 033508 (2021).

[98] H. Yuan and C.-H. Fred Fung, HOptimal Feedback Scheme and Universal Time Scaling for Hamiltonian Parameter Estimation, Phys. Rev. Lett. **115**, 110401 (2015).

[99] Z. Hou, Y. Jin, H. Chen, J.-F. Tang, C.-J. Huang, H. Yuan, G.-Y. Xiang, C.-F. Li, and G.-C. Guo, "Super-Heisenberg" and Heisenberg Scalings Achieved Simultaneously in the Estimation of a Rotating Field, Phys. Rev. Lett. **126**, 070503 (2021).

[100] U. Mishra and A. Bayat, Driving Enhanced Quantum Sensing in Partially Accessible Many-Body Systems, Phys. Rev. Lett. **127**, 080504 (2021).

[101] U. Mishra and A. Bayat, Integrable quantum many-body sensors for ac field sensing, arXiv:2105.13507 [quant-ph].

[102] J. Suzuki, Nuisance parameter problem in quantum estimation theory: Tradeoff relation and qubit examples, J. Phys. A: Math. Theor. **53**, 264001 (2020).

[103] J. S. Restrepo, Theory of quantum optomechanics with unconventional nonlinear coupling schemes, Ph.D. thesis, Université Paris 7, Sorbonne Paris Cité, 2014.

[104] D. F. Walls and G. J. Milburn, *Quantum Optics*, springer study ed. (Springer-Verlag, Berlin/New York, 1995).

[105] T. Niemczyk, F. Deppe, H. Huebl, E. P. Menzel, F. Hocke, M. J. Schwarz, J. J. Garcia-Ripoll, D. Zueco, T. Hümmer, E. Solano, A. Marx, and R. Gross, Circuit quantum electrodynamics in the ultrastrong-coupling regime, Nat. Phys. **6**, 772 (2010).

[106] K. W. Murch, K. L. Moore, S. Gupta, and D. M. Stamper-Kurn, Observation of quantum-measurement backaction with an ultracold atomic gas, Nat. Phys. **4**, 561 (2008).

[107] André Xuereb, C. Genes, and Aurélien Dantan, Strong Coupling and Long-Range Collective Interactions in Optomechanical Arrays, Phys. Rev. Lett. **109**, 223601 (2012).

[108] H. Kaviani, C. Healey, M. Wu, R. Ghobadi, A. Hryciw, and P. E. Barclay, Nonlinear optomechanical paddle nanocavities, Optica **2**, 271 (2015).

[109] M. R. Vanner, I. Pikovski, G. D. Cole, M. S. Kim, Č. Brukner, K. Hammerer, G. J. Milburn, and M. Aspelmeyer, Pulsed quantum optomechanics, Proc. Natl. Acad. Sci. U.S.A. **108**, 16182 (2011).

[110] M. L. Juan, G. Molina-Terriza, T. Volz, and O. Romero-Isart, Near-field levitated quantum optomechanics with nanodiamonds, Phys. Rev. A **94**, 023841 (2016).

[111] A. Ferraro, S. Olivares, and M. G. A. Paris, Gaussian states in continuous variable quantum information, arXiv:quant-ph/0503237.

[112] L. Neumeier and D. E. Chang, Exploring unresolved sideband, optomechanical strong coupling using a single atom coupled to a cavity, New J. Phys. **20**, 083004 (2018).

[113] J. D. Thompson, T. G. Tiecke, N. P. de Leon, J. Feist, A. V. Akimov, M. Gullans, A. S. Zibrov, V. Vuletić, and M. D. Lukin, Coupling a single trapped atom to a nanoscale optical cavity, Science **340**, 1202 (2013).

[114] B. Brandstätter, A. McClung, K. Schüppert, B. Casabone, K. Friebe, A. Stute, P. O. Schmidt, C. Deutsch, J. Reichel, R. Blatt, and T. E. Northup, Integrated fiber-mirror ion trap for strong ion-cavity coupling, Rev. Sci. Instrum. **84**, 123104 (2013).

[115] T. Ramos, V. Sudhir, K. Stannigel, P. Zoller, and T. J. Kippenberg, Nonlinear Quantum Optomechanics via Individual Intrinsic Two-Level Defects, Phys. Rev. Lett. **110**, 193602 (2013).

[116] L. Ding, C. Baker, P. Senellart, A. Lemaitre, S. Ducci, G. Leo, and I. Favero, High Frequency GaAs Nano-Optomechanical Disk Resonator, Phys. Rev. Lett. **105**, 263903 (2010).

[117] E. Peter, P. Senellart, D. Martrou, A. Lemaître, J. Hours, J. M. Gérard, and J. Bloch, Exciton-Photon Strong-Coupling Regime for a Single Quantum Dot Embedded in a Microcavity, Phys. Rev. Lett. **95**, 067401 (2005).

[118] P. Rabl, Photon Blockade Effect in Optomechanical Systems, Phys. Rev. Lett. **107**, 063601 (2011).

[119] T. Holz, R. Betzholz, and M. Bienert, Suppression of rabi oscillations in hybrid optomechanical systems, Phys. Rev. A **92**, 043822 (2015).

[120] S. Asiri, W. Ge, and M. S. Zubairy, Optomechanically induced anomalous population inversion in a hybrid system, J. Phys. A: Math. Theor. **51**, 414017 (2018).

[121] W. Ge and M. S. Zubairy, Macroscopic optomechanical superposition via periodic qubit flipping, Phys. Rev. A **91**, 013842 (2015).

[122] C. Ventura-Velázquez, B. M. Rodríguez-Lara, and H. M. Moya-Cessa, Operator approach to quantum optomechanics, Phys. Scr. **90**, 068010 (2015).